Syndecan-4 tunes cell mechanics by activating the kindlin-integrin-RhoA pathway

Antonios Chronopoulos[1†], Stephen D. Thorpe[2†]*, Ernesto Cortes[1], Dariusz Lachowski[1], Alistair J. Rice[1], Vasyl V. Mykuliak[3,4], Tomasz Róg[5], David A. Lee[2], Vesa P. Hytönen[3,4]*, Armando E. del Río Hernández[1]*

[1]Cellular and Molecular Biomechanics Laboratory, Department of Bioengineering, Imperial College London, London, United Kingdom

[2]Institute of Bioengineering, School of Engineering and Materials Science, Queen Mary University of London, London, United Kingdom

[3]Faculty of Medicine and Health Technology and BioMediTech, Tampere University, Tampere, Finland

[4]Fimlab Laboratories, Tampere, Finland

[5]Department of Physics, University of Helsinki, Helsinki, Finland

[†]These authors contributed equally: Antonios Chronopoulos, Stephen D. Thorpe.

*Corresponding authors:

Armando E. del Río Hernández

Email: a.del-rio-hernandez@imperial.ac.uk

Vesa P. Hytönen

Email: vesa.hytonen@tuni.fi

Stephen D. Thorpe

Email: s.thorpe@qmul.ac.uk

Abstract

Extensive research over the past decades has identified integrins to be the primary transmembrane receptors that enable cells to respond to external mechanical cues. We reveal here a mechanism whereby syndecan-4 tunes cell mechanics in response to localised tension via a coordinated mechanochemical signalling response that involves activation of two other receptors: epidermal growth factor receptor, and β1 integrin. Tension on syndecan-4 induces cell-wide activation of the kindlin-2/β1 integrin/RhoA axis in a PI3K dependent manner. Furthermore, syndecan-4 mediated tension at the cell-extracellular matrix interface is required for YAP activation. Extracellular tension on syndecan-4 triggers a conformational change in the cytoplasmic domain, the variable region of which is indispensable for the mechanical adaptation to force, facilitating the assembly of a syndecan-4/α-actinin/F-actin molecular scaffold at the bead adhesion. This mechanotransduction pathway for syndecan-4 should have immediate implications for the broader field of mechanobiology.

Keywords: syndecan-4, mechanotransduction, mechanobiology, integrin, kindlin, alpha-actinin, F-actin, RhoA, PI3K, YAP.

Syndecans belong to a family of four transmembrane proteoglycan adhesion receptors. Among them, syndecan-4 is the only family member that is ubiquitously expressed across nucleated cells and enriched in focal adhesions[1]. The extracellular domain of syndecan-4 bears heparan sulphate chains that bind to ECM proteins containing heparin binding domains (e.g. fibronectin) in addition to growth factors[2]. The transmembrane domain drives dimerization, and the cytoplasmic domain promotes binding to focal adhesion components and intracellular kinases[3]. Syndecan-4 acts synergistically with integrins to regulate substrate adhesion, focal adhesion assembly and cytoskeletal organisation[3-5]. Syndecan-4 also complexes with integrin $\alpha_5\beta_1$ to cooperatively bind Thy-1 (CD90), forming a unique dynamic catch bond which strengthens under force to mediate adhesion signalling[6]. Much like integrins, syndecan-4 provides a direct mechanical linkage from the extracellular matrix (ECM) to the actin cytoskeleton and is thus well positioned to support force transmission and act as a mechanotransducer.

Syndecan-4 null mice exhibit delayed wound healing[7], while syndecan-4 null cells show impaired contractility, cytoskeletal organisation, and immature focal adhesions[8-12], all suggestive of mechanosensation deficits. Indeed, studies in endothelial cells under fluid shear have implicated syndecan-4 in mechanotransduction both *in vitro*[13,14] and *in vivo*[15,16]. Syndecan-4 has additionally been shown to respond to directly applied mechanical tension, activating mitogen-activated protein kinase (MAPK) and protein kinase C-α (PKC-α) signalling[17,18]. These studies suggest syndecan-4 is directly involved in mechanotransduction, however its specific role and the underlying molecular mechanisms are unknown. Here, we have combined biophysical, cell biology and computational techniques to reveal a role for syndecan-4 in regulating cell mechanics through a previously unidentified mechanotransduction pathway requiring synergistic integrin activation.

Results

Tension on syndecan-4 induces adaptive cell stiffening

Tensional force on mechanosensitive receptors, such as integrins, triggers rapid cytoskeletal remodelling and adaptive cellular stiffening[19]. This response has also been observed in cell-cell junction proteins, E-cadherin and platelet endothelial cell adhesion molecule-1 (PECAM-1)[20,21], and nuclear envelope component nesprin-1[22]. To investigate if syndecan-4 acts as a mechanotransducer, we used electromagnetic tweezers to apply repeated localised mechanical tension to the syndecan-4 receptor on cells plated on fibronectin via ligand-coated magnetic beads, while tracking bead displacement (Fig. 1a). To ensure specificity of the cellular response to force, we coated the magnetic beads with an anti-syndecan-4 antibody (Anti-Sdc4) that binds specifically to the ectodomain of syndecan-4 core protein (Supplementary Figs. 1,2). Application of 12 successive 1 nN force pulses to Anti-Sdc4 beads triggered an adaptive increase in cellular stiffness evident as a decrease in bead displacement, reaching a relative displacement reduction of 37% by the 12th pulse (Fig. 1b,c, Supplementary Fig. 3). To mimic physiological ligand binding to the heparan sulphate chains of syndecan-4, we used beads coated with the 40 kDa α-chymotryptic fragment of fibronectin which contains the CS-1 heparin binding domain (FN-HBD) and does not bind integrins[23]. In this case we also observed a reduction in the amplitude of bead oscillation (Fig. 1c). Binding to the heparan sulphate chains of syndecan-4 was also achieved using fibronectin coated beads which were treated with an anti-fibronectin antibody (clone 3E3) which blocks the RGD integrin binding site but leaves the heparin binding domain available[23]. Again, we observed a decrease in the amplitude of bead oscillation indicative of adaptive cell stiffening (Supplementary Fig. 5). To ensure this response is specific to syndecan-4, we used the same force protocol on beads coated with poly-L-lysine (PLL) which binds the cell membrane non-specifically via electrostatic interactions, and an antibody that binds the extracellular domain of transferrin receptor protein-1 (Anti-TfR1), previously shown to be non-responsive to tensional force[19]. A reduction in bead

4

displacement over the 12 pulses was not observed in either case (Fig. 1c). These results demonstrate that tensional force applied specifically to syndecan-4 core protein or its associated heparan sulphate chains leads to an adaptive cellular stiffening response.

Using a battery of pharmacological inhibitors, we mechanistically investigated this syndecan-4-mediated mechanotransduction response. Pre-treatment of cells with the F-actin polymerisation inhibitor latrunculin A prior to force application prevented the stiffening response, with no reduction in relative bead displacement by force pulse 12 (Fig. 1d). Likewise, pharmacological inhibition of Rho with C3 transferase or Rho-associated protein kinase (ROCK) with Y-27632 also blocked a reduction in bead displacement (Fig. 1d), demonstrating that a functional contractile cytoskeleton is required for syndecan-4 mediated cell stiffening. Phosphoinositide 3-kinase (PI3K) activation has been shown to play a role in cell-cell junction mediated cellular stiffening[20,21]. Intriguingly, syndecan-4 mediated stiffening also showed a dependency on PI3K, as treatment with the PI3K inhibitor LY-294002 abrogated the cell's mechanical adaptation to force (Fig. 1d). PI3K activation produces freely diffusible phosphatidylinositol-3,4,5-trisphosphate (PIP_3) that acts as a lipid second messenger to propagate signalling cascades throughout the cell[24]. A major downstream effector of PI3K/PIP_3 signalling is AKT. However, selective inhibition of AKT using SH-5 did not prevent cell stiffening in response to force (Fig. 1d), suggesting PI3K acts via an alternative mechanotransduction pathway.

We next investigated whether tension on syndecan-4 activates PI3K activity through the generation of PIP_3 in cells expressing a green fluorescent protein (GFP) reporter containing the pleckstrin homology (PH) domain of AKT (PH-AKT-GFP) which binds PIP_3. Sustained 1 nN tension for 60 s on syndecan-4 resulted in elevated PI3K activity apparent by the accumulation of PH-AKT-GFP around the bead (Fig. 1e). No such accumulation was observed with the same force applied to PLL-

coated beads (Supplementary Fig. 6), indicating that force-induced PI3K activation is specific to syndecan-4.

Receptor tyrosine kinases can activate PI3K in response to ligand stimulation[24]. Epidermal growth factor receptor (EGFR) is a receptor tyrosine kinase that is known to form a complex with syndecan-4[25]. Activated EGFR recruits GRB2-associated-binding protein 1 (GAB1), which becomes tyrosine phosphorylated at sites that recruit the SH2 domains of the PI3K p85 subunit, providing an indirect mechanism for EGFR to activate PI3K[26]. To investigate how tension on syndecan-4 regulates PI3K activity, we treated cells with the EGFR inhibitor Gefitinib prior to application of sustained tension to syndecan-4 bound beads; this treatment abolished cell stiffening (Supplementary Fig. 7). As EGFR can be activated by both ligand-dependent and -independent mechanisms, we treated PH-AKT-GFP expressing cells with a neutralising anti-EGF antibody which inhibits EGF ligand-dependent EGFR signalling[27]. This treatment prevented force induced PI3K activation (Fig. 1f) and these cells failed to exhibit a stiffening response (Supplementary Fig. 7) upon force application to syndecan-4. EGF has been shown to sensitise mechano-responsiveness by enhancing strain mediated mechanotransduction[28], and increasing rigidity sensing[29], while the dependence of adaptive stiffening on ligand activation of EGFR and PI3K is analogous to a mechanotransduction pathway mediated by E-cadherin[21]. Hence, ligand-dependent activation of EGFR may amplify syndecan-4 mechanotransduction to facilitate downstream PI3K signalling. Collectively, these results demonstrate that syndecan-4 is a cellular mechanotransducer that tunes cell mechanics in response to localised tension via an adaptive stiffening response involving EGFR and PI3K mediated regulation of cytoskeletal remodelling via Rho.

Tension on syndecan-4 drives cell-wide focal adhesion growth

Most ECM molecules contain binding sites for both integrins and syndecans and there is substantial evidence of a clear synergy between the two receptor families[4]. Cooperative signalling from both integrins and syndecans potentiates force transduction and is required for the assembly of focal adhesion complexes, associated stress fibre formation, regulation of cytoskeletal dynamics and directional migration[3-5,30].

We thus asked if localised tension on syndecan-4 can actively recruit focal adhesion proteins talin and kindlin under force. These two families of FERM-domain proteins bind the cytoplasmic tail of integrins, recruit cytoskeletal and signalling proteins involved in mechanotransduction and synergise to activate integrin binding to the extracellular matrix[31]. Anti-Sdc4 magnetic beads adhered to the apical surface of cells on fibronectin prior to treatment with PI3K inhibitor LY-294002 or vehicle (DMSO). Using a permanent magnet, a sustained ~200 pN tensile force was applied to syndecan-4 for 5 min (Fig. 2a). In the absence of force, talin-1 and kindlin-2 immunofluorescent staining around the bead was limited. With sustained force application to syndecan-4, both talin-1 and kindlin-2 were recruited to the bead adhesion leading to an approx. 2-fold increase in staining intensity (Vehicle, Fig. 2b,c). However, when PI3K was inhibited, talin-1 and kindlin-2 were not recruited (Fig. 2b,c).

When we assessed talin-1 and kindlin-2 localisation at the basal membrane where the cell contacts the fibronectin ECM, we found a cell-wide increase in the size and number of talin-1 and kindlin-2 containing focal adhesions after sustained force application to apical syndecan-4 (Vehicle, Fig. 2d,e). PI3K inhibition similarly abrogated the force-induced recruitment of talin-1 and kindlin-2 to focal adhesions at the basal surface (Fig. 2d,e). This implies that localised force on syndecan-4 triggers PI3K dependent, cell-wide activation and growth of talin-1 and kindlin-2 enriched focal

adhesions to induce a global cellular response even at sites distal from the point of force application.

PIP₃ binding to kindlin-2 mediates integrin activation

The cell-wide growth of talin-1 and kindlin-2 containing focal adhesions prompted us to investigate if force on syndecan-4 leads to inside-out activation of integrin receptors. Binding of the talin FERM domain to the β integrin tail provides one key activation signal, but kindlin-2 also plays a central role in this process[31]. Unlike talin, the FERM domain of kindlin-2 contains a PH domain with a binding site for PIP₃, which promotes talin-mediated integrin activation[32]. Biophysical induction of PI3K activity has been implicated in regulating integrin activation, although the molecular mechanisms have not been studied[20,21].

We used a permanent magnet to apply sustained ~200 pN tension for 5 min to syndecan-4 in cells plated on fibronectin. Total internal reflection fluorescence (TIRF) imaging of the basal surface of cells revealed a cell-wide activation of β1 integrins upon force application to syndecan-4, evident as an increase in the size of adhesions positive for the active conformation of integrin β1 (Fig. 3a,b). This is consistent with our findings showing PI3K-dependent cell-wide growth of kindlin-2 and talin-1 enriched focal adhesions (Fig. 2d,e). The force-induced increase of activated β1 integrins mirrored the levels induced by Mn^{2+} treatment (without force), which shifts integrins into a high-affinity conformation, whereas removal of divalent cations with EDTA treatment reduced β1 integrin activation (Fig. 3a,b). We observed no change in the levels of total integrin β1 incorporation into adhesions under the same conditions (Supplementary Fig. 8).

Biochemical and structural studies have affirmed that the interaction of PIP₃ with kindlin-2 is critical to regulating the latter's function by promoting membrane anchoring and integrin

activation[32,33]. We thus asked whether force on syndecan-4 regulates integrin activation through an interaction between kindlin-2 and PIP$_3$. siRNA-mediated knockdown of kindlin-2 suppressed the previously observed activation of β1 integrins under force (Fig. 3c,d). Re-expression of a kindlin-2 mutant (K390A), lacking phosphoinositide binding activity[34], into kindlin-2 knockdown cells failed to recover cell-wide activation of β1 integrins in response to tension on syndecan-4 (Fig. 3c,d, Supplementary Fig. 9). Force-induced activation of β1 integrins was rescued in kindlin-2 knockdown cells re-expressing wild type kindlin-2. Collectively, these results indicate that activation of PI3K in response to localised tension on syndecan-4 triggers cell-wide inside-out activation of β1 integrins through PIP$_3$ interaction with kindlin-2 at focal adhesions.

RhoA activation requires additional ECM-integrin ligation

While we have shown that Rho is required for syndecan-4 mediated adaptive cell stiffening (Fig. 1d), the role that RhoA plays in this syndecan-4 mediated mechanotransduction pathway remains unclear. For this reason, we measured activation levels of RhoA and found that sustained ~200 pN tensional force on syndecan-4 increased RhoA activation in a time-dependent manner (Fig. 4a). We next sought to determine whether the observed cell-wide basal activation of β1 integrins and growth of focal adhesions is a consequence, or an essential element in the syndecan-4 mechanotransduction cascade leading to adaptive cell stiffening. Syndecan-4 is known to work in concert with integrins to regulate focal adhesion growth and cytoskeletal organisation[4]. Thus, we investigated whether force-induced RhoA activation and adaptive cell stiffening downstream of tension on syndecan-4 requires engagement of integrins.

Fibronectin contains domains that can engage both integrins and syndecans via their heparan sulphate chains. The integrin-binding domain of fibronectin lies within the 10th type III module (FN-III$_{10}$) containing the Arg-Gly-Asp (RGD) motif, while the heparin binding domain lies within

9

type III repeats 12-14 (FN-III$_{12-14}$). We thus treated cells adherent to fibronectin with an anti-fibronectin antibody (clone 3E3) which blocks the RGD integrin binding site in FN-III$_{10}$ (ref. 23) to prevent integrin ligation and the formation of new fibronectin connections. We applied a 1 nN pulsatile force to syndecan-4 and observed adaptive cell stiffening in the presence of an isotype control IgG1-κ antibody (Fig. 4b). However, blocking the integrin-binding domain of fibronectin (Anti-FN 3E3 Ab) inhibited the stiffening response (Fig. 4b); suggesting that syndecan-4 mediated force transduction requires engagement of new β1 integrins with the underlying fibronectin substrate. Indeed, when syndecan-4 on cells in the presence of the same antibodies was subjected to sustained force of ~200 pN for 5 min using a permanent magnet, immunofluorescent staining revealed enhanced engagement of new β1 integrins in the presence of the IgG control antibody which did not occur when the RGD integrin binding site was blocked (Anti-FN 3E3 Ab; Fig 4c,d). Consistent with this, blocking of fibronectin's RGD integrin binding site also suppressed RhoA activation upon sustained force application on syndecan-4 (Fig. 4e). No changes in cell spread area were observed upon blocking of the RGD integrin binding site (Supplementary Fig. 11). Analogous but slightly attenuated adaptive stiffening and RhoA responses were observed in cells on collagen type I (Supplementary Fig. 12), indicating that RGD-specific integrin ligation is not a requirement for RhoA induction. These results demonstrate that activation of RhoA in response to tension on syndecan-4 requires the engagement of new integrin-ECM connections.

Syndecan-4 mediated tension regulates YAP activation

RhoA activity and cytoskeletal tension are known actors in various mechanotransduction pathways which lead to changes in gene expression impacting cell function[35]. Yes-associated protein (YAP) is a transcription coactivator with a well-established role in converting biophysical inputs into gene expression signatures[36]. We sought to investigate whether syndecan-4 modulates YAP activity to regulate gene expression and cell function.

Wild-type (WT) and syndecan-4 null (Sdc4-/-) mouse embryonic fibroblasts (MEFs) were plated onto fibronectin-coated glass or 25 kPa polyacrylamide gels. WT cells adopted a spread morphology with prominent F-actin stress fibres and a high nuclear:cytoplasmic YAP ratio (Fig. 4f,g, Supplementary Fig. 13). In contrast, YAP was mostly cytoplasmic in Sdc4-/- cells, and while these cells adhered and spread as normal, they lacked F-actin stress fibres, suggestive of lower cytoskeletal tension (Fig. 4f,g, Supplementary Fig. 13). Nuclear localisation of YAP could be partially rescued with the expression of WT syndecan-4-GFP in Sdc4-/- cells (Fig. 4f,g). These syndecan-4 dependent changes in YAP activity altered the mRNA expression of established YAP target genes as both connective tissue growth factor (*Ctgf*) and ankyrin repeat domain 1 (*Ankrd1*) were found to be downregulated in Sdc4-/- cells compared to WT cells (Fig. 4h).

The role of syndecan-4 in the regulation of YAP activity is not limited to fibronectin, as we also observed a reduction in the ratio of nuclear:cytoplasmic YAP in Sdc4-/- compared to WT cells when plated on collagen type I (Supplementary Fig. 14). Consistent with the attenuated syndecan-4 force mediated cell-stiffening and RhoA activation observed in cells on collagen type I as opposed to fibronectin, both WT and Sdc4-/- cells exhibited decreased nuclear:cytoplasmic YAP on collagen type I compared to fibronectin (Supplementary Fig. 14). These results suggest that syndecan-4-mediated tension at the cell-ECM interface is essential for YAP transcriptional signalling.

Syndecan-4's V-region is required for mechanotransduction
We next sought to identify the molecular mechanism through which tension applied to the extracellular domain of syndecan-4 provokes a mechanoresponse. The cytoplasmic domain of syndecan-4 regulates interactions with scaffolding and signalling proteins and likely plays a role in mediating syndecan-4 mechanotransduction. It comprises a pair of conserved (C1 and C2) regions

11

common to all syndecan isoforms, separated by a variable (V) region specific to syndecan-4 (Fig. 5a).

Induction of protein phosphorylation is one of the first events that occurs when mechanical force is applied to cells[37]. We investigated the tyrosine residue Y180 in the C1 region of syndecan-4 which has been identified as a major phosphorylation site controlling integrin trafficking, focal adhesion dynamics and migratory behaviour[30]. Pulsatile 1 nN tension was applied to syndecan-4 bound beads attached to MEFs expressing either a syndecan-4 mutant which could not be phosphorylated on Y180 (Sdc4Y180L), or a phospho-mimetic syndecan-4 that emulates c-Src-mediated phosphorylation of the Y180 residue (Sdc4Y180E, Fig. 5b)[30]. The observed reduction in relative bead displacement demonstrated that both phospho-null Sdc4Y180L and phospho-mimetic Sdc4Y180E cells were able to stiffen under force; indicating that the phosphorylation status of Y180 is dispensable for syndecan-4 mechanotransduction (Fig. 5c).

The conserved C2 domain contains a PDZ-binding site that interacts with PDZ-domain containing proteins, which coordinate receptor clustering, exosome biogenesis and the formation of connections to the actin cytoskeleton, mainly via calcium/calmodulin-dependent serine protein kinase (CASK)[38,39]. We expressed a truncated syndecan-4 core protein lacking the C-terminal C2 (EFYA) domain (Sdc4Δ195E, Fig. 5b, Supplementary Fig. 16) in syndecan-4 null MEFs. Deletion of the C2 domain had no discernible effect on syndecan-4 mediated cell stiffening (Fig. 5c).

The syndecan-4 specific V-region interacts with both PKC-α and the phospholipid phosphatidylinositol (4,5) bisphosphate (PIP$_2$) to transduce downstream signals for cytoskeletal organisation[39,40]. The V-region further associates with the actin-crosslinking protein α-actinin to provide a direct mechanical link to the cytoskeleton[41]. MEFs expressing a syndecan-4 core protein

12

truncated in the centre of the V-region (Sdc4Δ187I, Fig. 5b, Supplementary Fig. 16) were unable to mount a stiffening response upon mechanical stimulation of syndecan-4 (Fig. 5c). The Sdc4Δ187I truncation deletes the binding site for PKC-α and α-actinin[41,42]. Previously, V-region truncation at this site has been associated with defects in cytoskeletal organisation, stress fibre assembly and focal adhesion formation, as well as inhibited myofibroblast differentiation[8,11]. As expected, adaptive cell stiffening was observed when tension was applied to MEFs expressing wild type syndecan-4 (Sdc4WT; Fig. 5c, Supplementary Fig. 16). These results indicate that interactions between the V-region of syndecan-4's cytoplasmic domain and its binding partners α-actinin and/or PKC-α is necessary to initiate mechanotransduction and mechanical adaptation to force.

External tension alters cytoplasmic syndecan-4 conformation

To investigate the effect of tensional force on syndecan-4 at the molecular level, we conducted molecular dynamics (MD) simulations. The system consisted of homodimeric transmembrane and cytoplasmic domains of syndecan-4 embedded within a membrane bilayer containing a mixture of lipids, including PIP_2. In equilibrium 50 ns MD simulations (no applied force) syndecan-4 structure showed no major conformational changes in the cytoplasmic domain (Fig. 5d). Constant force pulling at 50 pN applied to the extracellular side of syndecan-4 caused directed movement of the cytoplasmic domain towards the membrane (Fig. 5d). Root mean square fluctuations (RMSF) of Cα show that the transmembrane helices in the hydrophobic core of the membrane are mostly stable during the simulation while the C-terminal residues (C2 region) are more flexible (Fig. 5e,f). We chose the lysine residue K190, as one of the most stable positions in the V region, to monitor the conformational changes of the cytoplasmic domain on the membrane plane (Fig. 5g). Directed movement of the cytoplasmic domain led to association of syndecan-4 with the membrane, where electrostatic interactions between lysine residues and heads of PIP_2 lipids took place. Using constant force pulling at 50 pN and 100 pN over a 50 ns simulation, we observed similar tilting of the

cytoplasmic domain towards the plasma membrane (Supplementary Figs. 17,18). The use of 25 pN constant force caused a similar but slower conformational change within the cytoplasmic domain with 100 ns required to observe an effect like that seen at 50 ns under 50 pN. Using a higher force magnitude of 200 pN caused increased sliding of the protein through the membrane, resulting in non-directed movement of the cytoplasmic domain (Supplementary Fig. 18).

The observed force-dependent orientation of the cytoplasmic domain, leading to membrane interactions, may be important in the modulation of intracellular associations between syndecan-4 and its binding partners, including the scaffolding protein α-actinin which is known to interact with the region.

Force stabilises a syndecan-4/α-actinin/F-actin linkage

We next sought to investigate how the force-induced conformational change in the cytoplasmic V region is linked to syndecan-4 mechanosignalling. α-actinin, via spectrin repeat 4 (SR4) in its rod domain, interacts with syndecan-4's cytoplasmic V-region to establish a mechanical linkage between syndecan-4 and the actin cytoskeleton (Fig. 6a)[10]. We used siRNA to knockdown the endogenous expression of the predominant α-actinin isoforms — α-actinin-1 (*Actn1*) and α-actinin-4 (*Actn4;* si*Actn1Actn4*) — in MEFs, and subsequently expressed fluorescently tagged α-actinin-1 (ACTN1)-GFP which localised to focal adhesions throughout the cell (Supplementary Fig. 19). When 1 nN sustained tension was applied to syndecan-4 bound beads with magnetic tweezers, accumulation of ACTN1-GFP could be observed in a region of interest surrounding the magnetic bead after 60 s (Fig. 6b,c).

Further to this finding, MEFs with siRNA-mediated knockdown of α-actinin-1 and -4 (si*Actn1Actn4*) were unable to exhibit an adaptive stiffening response to 1 nN pulsatile tension

applied on syndecan-4 (Fig. 6d). While adaptive stiffening could be rescued through re-expression of full length ACTN1-GFP into α-actinin depleted cells (si*Actn1Actn4* + ACTN1-GFP), re-expression of an α-actinin mutant, where the actin-binding domain (ABD) was deleted (si*Actn1Actn4* + ACTN1-ΔABD-GFP)[43], failed to rescue the adaptive stiffening response to tension on syndecan-4 (Fig. 6d). Cells transfected with non-targeting control siRNA (siNT) maintained the adaptive stiffening response (Fig. 6d).

These results imply that force on syndecan-4 stabilises the assembly of a syndecan-4/α-actinin/F-actin molecular scaffold at the cell-ECM junction to facilitate force transmission and downstream syndecan-4 mechanosignalling (Fig. 6e).

Discussion

It has previously been reported that syndecan-4 can initiate mechanochemical signalling without the need for other ECM receptors, exhibiting vinculin recruitment and activation of ERK[17] and PKC-α[18]. Syndecan-4 is also implicated in flow sensing in endothelial cells that ultimately confers atheroprotective effects[15,16]. We provide evidence that while syndecan-4 is capable of initiating mechanotransduction as a lone ECM receptor, the underlying signalling network integrates distinct plasma membrane receptors; EGFR which augments the mechanoresponse and β1 integrins which are required for adaptive cellular stiffening. Our results demonstrate that localised tension on syndecan-4 initiates an adaptive stiffening response through a mechanosignalling cascade that requires synergistic cell-wide activation of β1 integrins and formation of new integrin-ECM connections, followed by subsequent RhoA induced actomyosin contractility. We have established a force-dependent syndecan-integrin crosstalk with these two mechanosensors acting synergistically to induce RhoA activation, adaptive stiffening and YAP transcriptional signalling.

While adaptive cell stiffening and local adhesion strengthening are common mechanosensitive responses shared among integrins and cadherins, perhaps the most striking aspect of syndecan-4 mechanosensing is how a localised force can elicit a cell-wide response as evidenced by the global growth of focal adhesions and activation of integrins. Intriguingly, our data suggest syndecan-4 mechanosignalling is both chemically and mechanically propagated throughout the cell via diffusion of PIP_3 lipid second messengers and mechanical transmission through the tensile cytoskeleton via a syndecan-4/α-actinin/F-actin molecular scaffold. This contrasts with the localised stiffening response which occurs when force is applied to integrin adhesions.

The dependence of adaptive stiffening on PI3K and integrins parallels in many ways the mechanotransduction pathways mediated by PECAM-1 in endothelia[20] and E-cadherin in epithelia[21]. Localised tension on PECAM-1 elicits a cell-wide mechanotransduction response[20], which is mediated by a mechanosensory complex additionally comprising vascular endothelial cell (VE-) cadherin and vascular endothelial growth factor receptor 2 (VEGFR2) which activates PI3K[44]. The analogous global mechanotransduction response observed for these distinct mechanoreceptors—syndecan-4, PECAM-1 and E-cadherin—suggests that the kindlin-integrin-RhoA pathway leading to adaptive cell stiffening may be a conserved mechanism employed by numerous mechanosensory complexes.

The role of integrin-mediated mechanosignalling has been the subject of intense investigation, however a more integrative approach that includes syndecan-4 as a mechanosensor could unearth new disease mechanisms. In summary, our results suggest that syndecan-4 is a key cellular mechanotransducer that responds to localised mechanical tension by eliciting a global response that regulates cell mechanics via cell-wide engagement of a PIP_3/kindlin-2/integrin/RhoA axis as well as

16

serving as a potent modulator of YAP activity with important implications for

mechanotransduction, syndecan biology, and cell-ECM interactions.

References

1   Kim, C. W., Goldberger, O. A., Gallo, R. L. & Bernfield, M. Members of the syndecan family of heparan sulfate proteoglycans are expressed in distinct cell-, tissue-, and development-specific patterns. *Mol. Biol. Cell* **5,** 797-805 (1994).

2   Elfenbein, A. & Simons, M. Syndecan-4 signaling at a glance. *J. Cell Sci.* **126,** 3799-3804 (2013).

3   Okina, E., Manon-Jensen, T., Whiteford, J. R. & Couchman, J. R. Syndecan proteoglycan contributions to cytoskeletal organization and contractility. *Scand. J. Med. Sci. Sports* **19,** 479-489 (2009).

4   Morgan, M. R., Humphries, M. J. & Bass, M. D. Synergistic control of cell adhesion by integrins and syndecans. *Nat. Rev. Mol. Cell Biol.* **8,** 957-969 (2007).

5   Saoncella, S. *et al.* Syndecan-4 signals cooperatively with integrins in a Rho-dependent manner in the assembly of focal adhesions and actin stress fibers. *Proc. Natl. Acad. Sci. USA* **96,** 2805-2810 (1999).

6   Fiore, V. F., Ju, L., Chen, Y., Zhu, C. & Barker, T. H. Dynamic catch of a Thy-1-alpha5beta1+syndecan-4 trimolecular complex. *Nat. Commun.* **5,** 4886 (2014).

7   Echtermeyer, F. *et al.* Delayed wound repair and impaired angiogenesis in mice lacking syndecan-4. *J. Clin. Invest.* **107,** R9-R14 (2001).

8   Longley, R. L. *et al.* Control of morphology, cytoskeleton and migration by syndecan-4. *J. Cell Sci.* **112,** 3421-3431 (1999).

9   Cavalheiro, R. P. *et al.* Coupling of vinculin to F-actin demands Syndecan-4 proteoglycan. *Matrix Biol.* **63,** 23-37 (2017).

10   Okina, E., Grossi, A., Gopal, S., Multhaupt, H. A. & Couchman, J. R. Alpha-actinin interactions with syndecan-4 are integral to fibroblast-matrix adhesion and regulate cytoskeletal architecture. *Int. J. Biochem. Cell Biol.* **44,** 2161-2174 (2012).

11   Gopal, S. *et al.* Heparan sulfate chain valency controls syndecan-4 function in cell adhesion. *J. Biol. Chem.* **285,** 14247-14258 (2010).

12   Chen, Y. *et al.* Matrix Contraction by Dermal Fibroblasts Requires Transforming Growth Factor-β/Activin-Linked Kinase 5, Heparan Sulfate-Containing Proteoglycans, and MEK/ERK. *Am. J. Pathol.* **167,** 1699-1711 (2005).

13   Florian, J. A. *et al.* Heparan sulfate proteoglycan is a mechanosensor on endothelial cells. *Circ. Res.* **93,** e136-142 (2003).

14   Moon, J. J. *et al.* Role of cell surface heparan sulfate proteoglycans in endothelial cell migration and mechanotransduction. *J. Cell. Physiol.* **203,** 166-176 (2005).

15   Baeyens, N. *et al.* Syndecan 4 is required for endothelial alignment in flow and atheroprotective signaling. *Proc. Natl. Acad. Sci. USA* **111,** 17308-17313 (2014).

16   Wang, Y. *et al.* Syndecan 4 controls lymphatic vasculature remodeling during mouse embryonic development. *Development* **143,** 4441-4451 (2016).

17   Bellin, R. M. *et al.* Defining the role of syndecan-4 in mechanotransduction using surface-modification approaches. *Proc. Natl. Acad. Sci. USA* **106,** 22102-22107 (2009).

18   Huang, C.-P., Cheng, C.-M., Su, H.-L. & Lin, Y.-W. Syndecan-4 Promotes Epithelial Tumor Cells Spreading and Regulates the Turnover of PKCalpha Activity under Mechanical Stimulation on the Elastomeric Substrates. *Cell. Physiol. Biochem.* **36,** 1291-1304 (2015).

19   Guilluy, C. *et al.* The Rho GEFs LARG and GEF-H1 regulate the mechanical response to force on integrins. *Nat. Cell Biol.* **13,** 722-727 (2011).

20   Collins, C. *et al.* Localized tensional forces on PECAM-1 elicit a global mechanotransduction response via the integrin-RhoA pathway. *Current biology : CB* **22,** 2087-2094 (2012).

21   Muhamed, I. *et al.* E-cadherin-mediated force transduction signals regulate global cell mechanics. *J. Cell Sci.* **129,** 1843-1854 (2016).

22   Guilluy, C. *et al.* Isolated nuclei adapt to force and reveal a mechanotransduction pathway in the nucleus. *Nat. Cell Biol.* **16,** 376-381 (2014).

23   Pierschbacher, M. D., Hayman, E. G. & Ruoslahti, E. Location of the cell-attachment site in fibronectin with monoclonal antibodies and proteolytic fragments of the molecule. *Cell* **26,** 259-267 (1981).

24   Vanhaesebroeck, B., Guillermet-Guibert, J., Graupera, M. & Bilanges, B. The emerging mechanisms of isoform-specific PI3K signalling. *Nat. Rev. Mol. Cell Biol.* **11,** 329-341 (2010).

25   Wang, H., Jin, H. & Rapraeger, A. C. Syndecan-1 and Syndecan-4 Capture Epidermal Growth Factor Receptor Family Members and the alpha3beta1 Integrin Via Binding Sites in Their Ectodomains: NOVEL SYNSTATINS PREVENT KINASE CAPTURE AND INHIBIT alpha6beta4-INTEGRIN-DEPENDENT EPITHELIAL CELL MOTILITY. *J. Biol. Chem.* **290,** 26103-26113 (2015).

26   Lemmon, M. A. & Schlessinger, J. Cell signaling by receptor tyrosine kinases. *Cell* **141,** 1117-1134 (2010).

27   Sakaguchi, M. *et al.* S100A11, an dual mediator for growth regulation of human keratinocytes. *Mol. Biol. Cell* **19,** 78-85 (2008).

28   Muller-Deubert, S., Seefried, L., Krug, M., Jakob, F. & Ebert, R. Epidermal growth factor as a mechanosensitizer in human bone marrow stromal cells. *Stem Cell Res.* **24,** 69-76 (2017).

29   Saxena, M. *et al.* EGFR and HER2 activate rigidity sensing only on rigid matrices. *Nat. Mater.* **16,** 775-781 (2017).

30   Morgan, M. R. *et al.* Syndecan-4 phosphorylation is a control point for integrin recycling. *Dev. Cell* **24,** 472-485 (2013).

31   Calderwood, D. A., Campbell, I. D. & Critchley, D. R. Talins and kindlins: partners in integrin-mediated adhesion. *Nat. Rev. Mol. Cell Biol.* **14,** 503-517 (2013).

32   Liu, J. *et al.* Structural basis of phosphoinositide binding to kindlin-2 protein pleckstrin homology domain in regulating integrin activation. *J. Biol. Chem.* **286,** 43334-43342 (2011).

33   Liu, Y., Zhu, Y., Ye, S. & Zhang, R. Crystal structure of kindlin-2 PH domain reveals a conformational transition for its membrane anchoring and regulation of integrin activation. *Protein Cell* **3,** 434-440 (2012).

34   Qu, H. *et al.* Kindlin-2 regulates podocyte adhesion and fibronectin matrix deposition through interactions with phosphoinositides and integrins. *J. Cell Sci.* **124,** 879-891 (2011).

35   Vining, K. H. & Mooney, D. J. Mechanical forces direct stem cell behaviour in development and regeneration. *Nat. Rev. Mol. Cell Biol.* (2017).

36   Panciera, T., Azzolin, L., Cordenonsi, M. & Piccolo, S. Mechanobiology of YAP and TAZ in physiology and disease. *Nat. Rev. Mol. Cell Biol.* (2017).

37   Hoffman, B. D., Grashoff, C. & Schwartz, M. A. Dynamic molecular processes mediate cellular mechanotransduction. *Nature* **475,** 316-323 (2011).

38   Baietti, M. F. *et al.* Syndecan-syntenin-ALIX regulates the biogenesis of exosomes. *Nat. Cell Biol.* **14,** 677-685 (2012).

39   Bass, M. D. & Humphries, M. J. Cytoplasmic interactions of syndecan-4 orchestrate adhesion receptor and growth factor receptor signalling. *Biochem. J.* **368,** 1-15 (2002).

40   Dovas, A., Yoneda, A. & Couchman, J. R. PKCalpha-dependent activation of RhoA by syndecan-4 during focal adhesion formation. *J. Cell Sci.* **119,** 2837-2846 (2006).

41   Greene, D. K., Tumova, S., Couchman, J. R. & Woods, A. Syndecan-4 associates with alpha-actinin. *J. Biol. Chem.* **278,** 7617-7623 (2003).

42   Lim, S. T., Longley, R. L., Couchman, J. R. & Woods, A. Direct binding of syndecan-4 cytoplasmic domain to the catalytic domain of protein kinase C alpha (PKC alpha) increases focal adhesion localization of PKC alpha. *J. Biol. Chem.* **278,** 13795-13802 (2003).

43   Roca-Cusachs, P. *et al.* Integrin-dependent force transmission to the extracellular matrix by alpha-actinin triggers adhesion maturation. *Proc. Natl. Acad. Sci. USA* **110,** E1361-1370 (2013).

44   Tzima, E. *et al.* A mechanosensory complex that mediates the endothelial cell response to fluid shear stress. *Nature* **437,** 426-431 (2005).

Author contributions

A.C. and A.J.R. conducted magnetic tweezers experiments; A.C. and S.D.T. conducted permanent magnet experiments; S.D.T. and A.C. performed and analysed experiments with mouse embryonic fibroblast cells; A.C. E.C., D.L. and S.D.T. performed and analysed experiments with pancreatic stellate cells; S.D.T. carried out transfections, and western blots, and IF experiments supervised by D.A.L.; E.C. carried out RhoA activity experiments; V.V.M. performed MD and SMD experiments supervised by V.P.H. and T.R.; D.L. performed IF experiments and data analysis; A.C., S.D.T. and A.D.R.H. designed the studies, and wrote and prepared the manuscript with significant inputs from V.P.H.; all authors commented on the manuscript.

Competing financial interests

The authors declare no competing interests.

Methods

Cell culture and reagents

Primary human culture activated pancreatic stellate cells (PSCs; Caltag Medsystems SC-3830) were cultured at 37°C, 5% CO_2 in Dulbecco's modified Eagle's medium/F12 Ham (DMEM/F12; D8437) with 2% foetal bovine serum (FBS), 100 U ml^{-1} penicillin-100 µg ml^{-1} streptomycin (all Sigma-Aldrich) and 2.5 µg ml^{-1} amphotericin B (Gibco) and used at passage 4-8. Immortalised mouse embryonic fibroblast (MEF) cell lines were a gift from Dr Mark Morgan and included wild type, syndecan-4 -/- (ref. 45), and lines expressing mutant syndecan-4 phospho-null Y180L, and phospho-mimetic Y180E (ref. 30). MEFs were cultured at the large T-antigen permissive temperature of 33°C in high glucose DMEM (Gibco) with 10% FBS and 100 U ml^{-1} penicillin-100

μg ml^{-1} streptomycin (all Sigma-Aldrich). All experiments and treatments were conducted at 37°C. Cells were plated on substrates coated with 2.5 μg ml^{-1} fibronectin or 10 μg ml^{-1} collagen type I (Sigma-Aldrich). 25 kPa polyacrylamide gels were fabricated as described previously[46]. Expression of syndecan-4 in MEFs and PSCs was confirmed using western blot (Supplementary Fig. 22).

Cells were treated with 0.5 μM latrunculin A (Merck 428026) for 1 h to inhibit F-actin polymerisation, with 2 μg ml^{-1} C3 transferase (Cytoskeleton Inc.) for 4 h to inhibit Rho, with 10 μM Y-27632 (Merck 688001) for 1 h to inhibit ROCK, with 30 μM LY-294002 (Sigma Aldrich L9908) for 1 h to inhibit PI3K, with 10 μM SH-5 (Abcam ab141442) for 1 h to inhibit AKT, and with 15 μM Gefitinib (Santa Cruz Biotechnology sc-202166) for 2 h to inhibit EGFR. Cells were treated with 1 mM MnCl$_2$ (Fisher Scientific) for 30 min to induce integrin activation, and 2 mM EDTA (Sigma Aldrich) for 30 min to sequester divalent ions responsible for integrin activation. Cells were treated with 5 μg ml^{-1} mouse anti-human EGF antibody, clone 10825 (R&D Systems MAB236; RRID:AB_2095960) to neutralise EGF. Cells plated on fibronectin substrates were treated with 20 μg ml^{-1} mouse anti-fibronectin antibody (cell attachment fragment), clone 3E3 (Merck MAB88916; RRID:AB_95479), for 30 min to block integrin ligation to RGD. Mouse IgG1-κ, clone MOPC-21 (Merck MABF1081Z; RRID:AB_395252) was used as an isotype control.

PSCs were transfected by electroporation using the Neon Transfection system (Thermo Fisher Scientific) with one pulse of 1,300 V for 30 ms. WT and Sdc4-/- MEF cell lines were transfected using Lipofectamine 3000 (Thermo Fisher Scientific). After transfection, cells were allowed recover in antibiotic-free media for 24 h. Experiments were conducted 48 h post transfection. Cells were transfected with siRNA targeting kindlin-2 (*Mig-2*, sc-106786), both α-actinin-1 (*Actn1*, sc-43096) and α-actinin-4 (*Actn4*, sc-43102), or non-targeting control (sc-37007, all Santa Cruz

Biotechnology). The PH-AKT-GFP plasmid was a gift from Tamas Balla (Addgene plasmid 51465; RRID:Addgene_51465)[47]. The kindlin-2-GFP plasmid was a gift from Jun Qin[32]. The kindlin-2-K390A-HA plasmid lacking phosphoinositide binding activity was a gift from Chuanyue Wu[34]. The syndecan-4 C2 truncation plasmid Sdc4Δ195E (ref. 11) and the syndecan-4 V-domain truncation plasmid Sdc4Δ187I (ref. 8) were gifts from John Couchman. The α-actinin-1 (ACTN1)-GFP plasmid was a gift from Carol Otey (Addgene plasmid 11908; RRID:Addgene_11908)[48] and α-actinin-1 (ACTN1)-ΔABD-GFP (Addgene plasmid 66935; RRID:Addgene_66935) was as described previously[43]. Control empty vector pEGFP-N1 was from Clontech. siRNA mediated knockdown of kindlin-2 was confirmed with immunofluorescent staining (Supplementary Fig. 9) and knockdown of α-actinin confirmed using western blot against α-actinin-4 (Supplementary Fig. 19). Plasmid expression was assessed based on GFP signal or immunofluorescent staining for the HA tag (Supplementary Fig. 16).

Magnetic bead preparation

Antibodies and ECM ligands were coupled to 4.5 μm epoxide paramagnetic beads (Dynabeads M-450 Epoxy, Thermo Fisher Scientific) according to manufacturer's instructions. Beads were washed twice in 0.1 M sodium phosphate buffer, pH 7.4, before coupling with 40 μg antibody or ECM ligand per 8×10^7 beads in 0.1 M sodium phosphate buffer pH 7.4 for 30 min followed by addition of 0.1% bovine serum albumin (BSA) and further incubation for 16 h at room temperature with gentle rotation throughout. Beads were washed and subsequently stored in 0.1% BSA-phosphate buffered saline (PBS) pH 7.4 at 4°C. Beads were coated with mouse anti-syndecan-4 antibody, clone 5G9 (Santa Cruz Biotechnology sc-12766; RRID:AB_628314), poly-L-lysine, fibronectin (both Sigma-Aldrich), the 40 kDa α-chymotryptic fragment of fibronectin which contains the CS-1 heparin binding domain (Merck F1903), or mouse anti-transferrin receptor-1, clone 3B8 2A1 (CD71, Santa Cruz Biotechnology sc-32272; RRID:AB_627167). For experiments, ligand-coated magnetic beads

were resuspended in media and incubated with cells for 30 min at 37°C. Cells were briefly washed with PBS to remove unbound beads prior to force application. Syndecan-4 binding to functionalised beads was confirmed by immunofluorescent staining (Supplementary Fig. 1) and isolation of the bead adhesion complex in cell lysates and subsequent western blotting (Supplementary Fig. 2).

Force application to cell bound beads

A custom-built electromagnetic tweezers apparatus fitted to an inverted microscope (Eclpise Ti, Nikon) was used to apply controlled pulsatile forces to individual ligand-coated magnetic beads attached to cells plated onto fibronectin or collagen type I coated glass bottomed dishes (Fluorodish, World Precision Instruments). Application of the pulsatile regimen consisting of 12 pulses of 1 nN force for 3 s with intervening 4 s periods of relaxation was achieved through a LabVIEW interface (National Instruments). On force application, bead displacements were recorded with a high-speed CMOS camera (Andor Neo sCMOS, Oxford Instruments) at 50 Hz using a 40× 0.6 NA air objective (Nikon). Displacement was tracked using a custom-written particle tracking algorithm in MATLAB that detects the intensity-weighted centroid of the bead with subpixel accuracy. The electromagnetic tweezers device was calibrated before the experiments using a fluid of known viscosity. Beads that showed displacements of less than 50 nm (detection resolution) and loosely bound beads were not selected for analysis. Application of sustained 1 nN force was also applied to cells for 60 s with concurrent imaging of GFP localisation around the attached bead. To apply a constant force on a larger number of beads, we used a permanent neodymium magnet that allowed us to apply a vertical tensile force on the beads with magnitudes of approx. 200 pN.

Immunofluorescent staining and image analysis

Cells were seeded on ECM coated coverslips for immunofluorescent staining. Following pertinent treatment, cells were fixed with 4% paraformaldehyde (Sigma-Aldrich P6148) in PBS for 10 min,

permeabilised with 0.1% Triton X-100 (Sigma, T8787) in PBS for 10 min and blocked with 5% donkey or goat serum in 1% BSA-PBS containing 0.01% Tween 20 (Sigma-Aldrich; PBST). In some cases, required primary antibodies were of the same species as the antibodies used to functionalise beads, or as treatment. To block secondary antibody binding to these sites, cells were incubated with an excess of anti-mouse secondary antibody in 1% BSA-PBST for 1h followed by PBS washing prior to incubation with primary antibodies prepared in 1% BSA-PBST for 1 h at room temperature or overnight at 4°C. Cells were washed in PBST and incubated with donkey or goat Alexa Fluor conjugated secondary antibodies (1:1,000; Thermo Fisher Scientific) and phalloidin (1:40; Thermo-Fisher Scientific, or 1:1,000; Santa Cruz Biotechnology) in 1% BSA-PBST for 30 min to 1 h at room temperature. Finally, coverslips were washed in PBST, and nuclei stained with 1 μg ml^{-1} DAPI (Sigma Aldrich) prior to mounting using ProLong mounting reagent or mounted in ProLong containing DAPI (Thermo Fisher Scientific, P36931). Primary antibodies: rabbit anti-syndecan-4 (1:100; Abcam ab24511; RRID:AB_448112), mouse anti-integrin β1, clone A-4 (1:100; Santa Cruz Biotechnology sc-374429; RRID:AB_11012020), mouse anti-integrin β1, clone 12G10 (1:100; Santa Cruz Biotechnology sc-59827; RRID:AB_782089), rabbit anti-talin-1 (1:400; Abcam, ab71333; RRID:AB_2204002), mouse anti-kindlin-2, clone 3A3 (1:250; Merck MAB2617; RRID:AB_10631873), mouse anti-β1 integrins, active conformation, clone HUTS-4 (1:100; Merck MAB2079Z; RRID:AB_2233964), mouse anti-YAP, clone 63.7 (1:200; Santa Cruz Biotechnology sc-101199; RRID:AB_1131430), rabbit anti-GFP (1:2,000; Abcam ab6556; RRID:AB_305564), mouse anti-HA.11 epitope tag, clone 16B12 (1:1,000; Biolegend 901513; RRID:AB_2565335), mouse anti-α-actinin, clone BM-75.2 (1:200; Sigma Aldrich A5044; RRID:AB_476737).

Samples were imaged using epifluorescent microscopy (Leica DMI4000B, Leica DMi8, Nikon Eclipse Ti, AE31 Motic), total internal reflection fluorescence (TIRF) microscopy (Nikon Eclipse

Ti), confocal microscopy (Zeiss LSM 710, Nikon Eclipse Ti) or structured illumination microscopy (GE OMX) as indicated in figure legends. Image quantification was conducted using NIS Elements (Nikon) or Fiji (ImageJ, NIH)[49]. A region of interest (ROI) with inner diameter equal to the bead size and outer diameter 9 μm was used to quantify immunofluorescent staining or GFP intensity at the bead adhesion. In live GFP images, this was applied to a single epifluorescent image for each time point. For localisation of adhesion proteins to the bead in immunofluorescently stained cells, the location of the bead was first located in widefield mode, and then imaged using confocal microscopy with a z-spacing of 125 μm. Intensity within the ROI was summed through 5 z-sections expressed as mean fluorescent intensity. Focal adhesion size was assessed from TIRF microscopy images or confocal z-sections of the cell's basal surface. An intensity-based threshold was applied to images to isolate talin-1, kindlin-2 or active integrin β1 enriched focal adhesions from background for selection. To assess YAP nuclear:cytoplasmic ratio, DAPI stained nuclei were selected based on an intensity threshold which provided ROIs for each nucleus. Morphological outlines of cell area were manually traced on F-actin images providing ROIs for each cell. The nucleus ROI could be subtracted from the cell ROI to obtain the cytoplasmic ROI. The mean intensity within each ROI was used to calculate the YAP nuclear:cytoplasmic ratio.

RhoA activity assay

Total RhoA and active RhoA-GTP were quantified using total RhoA ELISA and active RhoA G-LISA assay kits (Cytoskeleton, Inc. BK150 and BK124) according to the manufacturer's instructions. Immediately after treatment, cells were rinsed with ice-cold PBS and homogenised in ice-cold lysis buffer. Protein was quantified and sample concentration adjusted to 0.5 mg ml^{-1}. For the G-LISA, binding buffer was added, and assays performed in triplicate using 1.5 μg protein per well. Target binding to the Rho GTP-binding protein coated well was facilitated by 30 min incubation at 4°C with shaking, followed by washing. For the ELISA, protein lysate was added to

wells coated with anti-Rho IgY antibody and incubated for 120 min at room temperature followed by washing. Antigen-presenting buffer was added for 2 min, removed, and samples incubated with the anti-RhoA antibody (1:250) for 45 min (G-LISA) or 1 h (ELISA) at room temperature. Samples were washed three times and incubated with HRP conjugated secondary antibody for 45 min or 1 h at room temperature. HRP detection reagent was added, samples incubated briefly, and absorbance measured at 490 nm.

Gene expression analysis

RNA was isolated using the RNeasy Mini Kit (Qiagen 74104). The High-Capacity RNA-to-cDNA Kit (Thermo Fisher Scientific 4387406) was used to reverse transcribe 1 μg of RNA. Real time RT-PCR was performed in a 20 μl reaction with 100 ng cDNA, 300 nM primers and SYBR Green PCR Master Mix (Applied Biosystems 4309155). Primer sequences were: connective tissue growth factor (*CTGF*): forward 5'-CATACTCCACAGAATTTAGCTC-3', reverse 5'-TTAAGAAGGGCAAAAAGTGC-3'; ankyrin repeat domain 1 (*ANKRD1*): forward 5'-TGAGTATAAACGGACAGCTC-3', reverse 5'-TATCACGGAATTCGATCTGG-3'; and glyceraldehyde 3-phosphate dehydrogenase (*GAPDH*): forward 5'-ACAGTTGCCATGTAGACC-3', reverse 5'-TTTTTGGTTGAGCACAGG-3'. Relative expression was determined using the $2^{-\Delta\Delta Ct}$ method with GAPDH used as endogenous control.

Molecular Dynamics (MD) and Steered Molecular Dynamics (SMD) simulations

In simulations, we used the syndecan-4 structure including transmembrane and cytoplasmic domains. The NMR structure of the cytoplasmic domain (ID 1EJP in protein data bank) was used, while the transmembrane domain was modelled with SWISS-MODEL tool using the NMR structure of the dimeric transmembrane domain of human glycophorin A (ID 1AFO in protein data bank) as a template. A lipid membrane with 40 % of POPC (144 residues), 15 % POPS (54

residues), 5 % PIP$_2$ (18 residues) and 40 % cholesterol (144 residues) was generated using Charmm-gui[50]. Embedding of protein into the membrane was performed by applying high lateral pressure on the system as described before[51]. All simulations were performed using Gromacs 2016.1 (ref. 52) at the Sisu supercomputer, CSC, Finland. All-atom OPLS-AA force field[53] and explicit TIP3P water model[54] in 0.15 M KCl neutral solution were used. Energy minimisation of the system was performed in 10,000 steps using the steepest descent algorithm. Equilibration of the system was performed in three phases using harmonic position restraints on lipid/cholesterol heads in the Z dimension and on all heavy atoms of protein. (1) NVT ensemble simulation was performed for 100 ps utilising the Berendsen weak coupling algorithm[55] at 100 K. (2) Next, the system was heated from 100 to 310 K with constant heating rate over 1 ns using an NPT ensemble at 1 bar, using the Berendsen algorithm to control both temperature and pressure. Semi-isotropic pressure coupling was used for all the simulations to control pressure in the XY plane (membrane plane) and in the Z dimension separately. Temperature coupling was applied separately for protein/membrane and solution parts. (3) The final equilibration phase was performed using NPT ensemble at 310 K and 1 bar using Nose-Hoover[56,57] and Parrinello-Rahman[58] algorithms, respectively. These conditions were used in all subsequent simulations. An integration time step of 2 fs was used in all the simulations. Equilibrium MD simulations (with no force applied) for 50 ns were conducted, considering the first 20 ns as a relaxation step. Hence, conformation of the system at 20 ns of the first run of equilibrium MD simulation was used as a starting structure for SMD simulations. The pulling vector was set between the membrane (centre of mass) and Cα of N-terminal residues of the protein. SMD simulations were performed with constant force pulling using different force regimes: 25 pN, 50 pN, 100 pN and 200 pN. Two simulations were conducted for 25 pN, 100 pN and 200 pN, and four simulations for equilibrium MD and SMD with 50 pN of constant force pulling. All the simulations were run for 50 ns, except SMD simulations with 25 pN which were run for 100 ns.

Statistical analysis

Statistical analyses were conducted using GraphPad Prism 8 (RRID:SCR_002798; GraphPad Inc.) or Minitab 18 (RRID:SCR_014483; Minitab Inc.). Data were generated from multiple experimental repeats each containing multiple biological and technical replicates. Details of data presentation, number of replicates, statistical tests and significance is denoted in the figure legends. Where datasets followed a parametric distribution, experimental groups were compared using two-sided two-sample or paired t-tests, or when multiple experimental variables, analysis of variance with Tukey pairwise comparisons. Where datasets were non-parametric, two-sided Mann-Whitney tests, or two-sided paired rank tests were used in place of two-sample and paired t-tests respectively. In the case of multiple experimental groups, non-parametric data was transformed to fit a parametric distribution using a Box-Cox transformation prior to analysis of variance and pairwise comparisons, or the Kruskal-Wallis test used. Non-parametric bead displacement data over successive force pulses was analysed using the Friedman test with Dunn pairwise comparisons. The significance level for all tests was set at 0.05.

Data availability

The data that support the findings of this study are available from the corresponding authors upon reasonable request.

Code Availability

MATLAB code used to track bead displacements in magnetic tweezers experiments is available from A.D.R.H. upon reasonable request. Code used in molecular dynamics simulations is available from V.P.H. upon reasonable request.

References

45   Bass, M. D. *et al.* Syndecan-4-dependent Rac1 regulation determines directional migration in response to the extracellular matrix. *J. Cell Biol.* **177,** 527-538 (2007).

46   Lachowski, D. *et al.* Substrate Rigidity Controls Activation and Durotaxis in Pancreatic Stellate Cells. *Sci. Rep.* **7,** 2506 (2017).

47   Várnai, P. & Balla, T. Visualization of Phosphoinositides That Bind Pleckstrin Homology Domains: Calcium- and Agonist-induced Dynamic Changes and Relationship to Myo-[3H]inositol-labeled Phosphoinositide Pools. *J. Cell Biol.* **143,** 501-510 (1998).

48   Edlund, M., Lotano, M. A. & Otey, C. A. Dynamics of α-actinin in focal adhesions and stress fibers visualized with α-actinin-green fluorescent protein. *Cell Motility* **48,** 190-200 (2001).

49   Schindelin, J. *et al.* Fiji: an open-source platform for biological-image analysis. *Nat. Methods* **9,** 676-682 (2012).

50   Jo, S., Kim, T., Iyer, V. G. & Im, W. CHARMM-GUI: a web-based graphical user interface for CHARMM. *J. Comput. Chem.* **29,** 1859-1865 (2008).

51   Javanainen, M. Universal Method for Embedding Proteins into Complex Lipid Bilayers for Molecular Dynamics Simulations. *J. Chem. Theory Comput.* **10,** 2577-2582 (2014).

52   Van Der Spoel, D. *et al.* GROMACS: fast, flexible, and free. *J. Comput. Chem.* **26,** 1701-1718 (2005).

53   Kaminski, G. A., Friesner, R. A., Tirado-Rives, J. & Jorgensen, W. L. Evaluation and reparametrization of the OPLS-AA force field for proteins via comparison with accurate quantum chemical calculations on peptides. *J. Phys. Chem. B* **105,** 6474-6487 (2001).

54   Jorgensen, W. L. & Madura, J. D. Quantum and statistical mechanical studies of liquids. 25. Solvation and conformation of methanol in water. *J. Am. Chem. Soc.* **105,** 1407-1413 (1983).

55   Berendsen, H. J. C., Postma, J. P. M., van Gunsteren, W. F., DiNola, A. & Haak, J. R. Molecular-Dynamics with Coupling to an External Bath. *J. Chem. Phys.* **81,** 3684-3690 (1984).

56   Hoover, W. G. Canonical dynamics: Equilibrium phase-space distributions. *Phys. Rev. A Gen. Phys.* **31,** 1695-1697 (1985).

57   Nosé, S. A unified formulation of the constant temperature molecular dynamics methods. *J. Chem. Phys.* **81,** 511-519 (1984).

58   Parrinello, M. & Rahman, A. Polymorphic Transitions in Single-Crystals - a New Molecular-Dynamics Method. *J. Appl. Phys.* **52,** 7182-7190 (1981).

Figure legends

Figure 1. Tension on syndecan-4 induces Rho-dependent adaptive stiffening mediated by EGFR and PI3K. a, Schematic representation of electromagnetic tweezers pulling on a ligand-coated magnetic bead bound to the apical cell surface. Inset depicts an anti-syndecan-4 antibody-coated bead binding to the extracellular domain of syndecan-4. **b,** Representative cell stiffening response apparent as a progressively diminishing bead displacement over 12 force pulses. Bead displacement at force pulse 1 and 12 is indicated. $n = 32$ cells. **c,** Relative displacement of beads bound to pancreatic stellate cells (PSCs) plated on fibronectin. Beads were functionalised with anti-syndecan-4 antibody (Anti-Sdc4; $n = 32$), the heparin binding domain fragment of fibronectin (FN-HBD; $n = 31$), poly-L-lysine (PLL; $n = 20$) or anti-transferrin receptor protein-1 antibody (Anti-TfR1; $n = 36$ cells). Displacement for all pulses was normalised to the average displacement of force pulse 1. Friedman test with Dunn pairwise comparisons: $*P \leq 0.0116$, $**P \leq 0.0041$, $***P < 0.0001$ vs force pulse 1. **d,** Relative syndecan-4 bound bead displacement at force pulse 1 and 12 in control PSCs ($n = 32$), or PSCs treated with latrunculin A (Lat A; $n = 20$), C3 transferase (C3; $n = 20$), Y-27632 (Y-27; $n = 20$), LY-294002 (LY-29; $n = 20$), or SH-5 ($n = 24$ cells). See Supplementary Fig. 4 for single cell data. Two-sided paired signed rank test: $**P = 0.002$, $***P < 0.0001$. Mean ± s.e.m. **e,f,** Syndecan-4 bound beads on cells expressing the PIP$_3$ biosensor PH-AKT-GFP were exposed to sustained tension of 1 nN for 60 s in untreated conditions (**e**) or in the presence of an epidermal growth factor (EGF) neutralising antibody (**f**). Representative confocal slice images of the area surrounding the bead pre (0 s) and post (60 s) force application. Mean PH-AKT-GFP fluorescent intensity, in a region of interest depicted by white dashed overlay, is presented relative to intensity prior to force application. See Supplementary Fig. 6 for control GFP data. Scale bar: 5 μm. $n_{(e)} = 24$, $n_{(f)} = 10$ cells. Two-sided paired signed rank test: $***P = 0.0002$, n.s. $P = 0.723$. Boxes represent median and interquartile range, whiskers extend to the max/min data points, individual values overlaid.

Figure 2. Tension on syndecan-4 leads to PI3K dependent cell-wide growth of focal adhesions.
a, Syndecan-4 bound beads on pancreatic stellate cells plated on fibronectin and pre-treated with vehicle (DMSO) or PI3K inhibitor LY-294002 were exposed to sustained tension of ~200 pN for 5 min using a permanent magnet. **b,** Representative confocal maximum projection images of talin-1 and kindlin-2 at the bead site. White dashed overlay depicts region of interest (ROI) surrounding bead used for intensity quantification. Scale bar 5 μm. **c,** Mean fluorescent intensity of talin-1 and kindlin-2 in a ROI surrounding the bead was summed from each confocal section and presented relative to each unstimulated control. $n_{Talin-1}$ = 8-12 cells ($n_{Vehicle-Control}$ = 12, $n_{Vehicle-Force}$ = 11, $n_{LY-294002-Control}$ = 9, $n_{LY-294002-Force}$ = 8), $n_{Kindlin-2}$ = 8-18 cells ($n_{Vehicle-Control}$ = 14, $n_{Vehicle-Force}$ = 18, $n_{LY-294002-Control}$ = 8, $n_{LY-294002-Force}$ = 8); two-sided two-sample t-test: **P = 0.0021, ***P = 0.0001, n.s. $P \geq$ 0.543. Mean ± s.e.m. **d,** Representative TIRF microscopy images of talin-1 and kindlin-2 enriched basal focal adhesions. Scale bar 5 μm, inset scale bar 1 μm. **e,** Mean area of talin-1 and kindlin-2 positive focal adhesions. $n_{Talin-1}$ = 10-16 cells ($n_{Vehicle-Control}$ = 15, $n_{Vehicle-Force}$ = 15, $n_{LY-294002-Control}$ = 10, $n_{LY-294002-Force}$ = 16) and $n_{Kindlin-2}$ = 12 cells with $\geq$ 5 focal adhesions measured per cell; general linear model for analysis of variance with Tukey pairwise comparisons: ***$P <$ 0.0001, n.s. $P \geq$ 0.9726. Boxes represent median and interquartile range, whiskers extend to the max/min data points, individual values overlaid.

Figure 3. Tension on syndecan-4 triggers cell-wide integrin activation via PIP₃ binding to kindlin-2. a, Representative TIRF microscopy images of active β1 integrins in the basal plane of pancreatic stellate cells in (i) unstimulated control conditions, (ii) in response to a sustained tension force of ~200 pN for 5 min applied to syndecan-4, (iii) with 1 mM MnCl₂ treatment for 30 min (Mn²⁺), and (iv) with 2 mM EDTA treatment for 30 min, both (iii and iv) in the absence of force application. **b,** Mean active integrin β1 focal adhesion (FA) area. $n_{Control}$ = 14, n_{Force} = 14, n_{Mn2+} = 46, n_{EDTA} = 86 cells. **c,** Representative TIRF microscopy images of active β1 integrins in response

to sustained tension on syndecan-4 in cells treated with siRNA targeting kindlin-2 (siKindlin-2), re-expressing a kindlin-2 mutant (K390A) which lacks phosphoinositide binding activity (siKindlin-2 + Kindlin-2 K390A), and re-expressing wild type (WT) kindlin-2. Scale bar 10 μm, inset scale bar 2 μm. **d,** Mean active integrin β1 focal adhesion (FA) area. $n_{siKindlin\text{-}2} = 14$, $n_{siKindlin\text{-}2 + Kindlin\text{-}2\,K390A} = 14$, $n_{siKindlin\text{-}2 + Kindlin\text{-}2\,WT\text{-}Control} = 196$, $n_{siKindlin\text{-}2 + Kindlin\text{-}2\,WT\text{-}Force} = 52$ cells with ≥ 5 focal adhesions measured per cell; two-sided Mann-Whitney test: $*P = 0.024$, $***P \leq 0.0002$, n.s. $P \geq 0.73$. Boxes represent median and interquartile range, whiskers extend to the max/min data points.

Figure 4. Tension on syndecan-4 activates RhoA via integrin ligation and regulates YAP activity. a, Pancreatic stellate cells (PSCs) on fibronectin were subjected to sustained tension of ~200 pN on syndecan-4 for 5-15 min, with total and active RhoA presented relative to unstimulated control. $n_{Control/5min/15min} = 9$, $n_{10min} = 6$ biologically independent samples; Kruskal-Wallis test with Dunn pairwise comparisons: $*P = 0.0104$, $***P < 0.0001$, n.s. $P = 0.823$. **b,** Relative syndecan-4 bound bead displacement in untreated control conditions ($n = 32$), with IgG1-κ isotype control antibody ($n = 15$), or with anti-fibronectin antibody (clone 3E3) which blocks the RGD binding site on fibronectin (Anti-FN 3E3 Ab, $n = 22$ cells). See Supplementary Fig. 10 for single cell data. Two-sided paired signed rank test: $*P = 0.035$, $***P < 0.0001$, n.s. $P = 0.134$. **c,** Representative confocal microscopy sections at the cell's basal surface for active β1 integrin and F-actin in response to sustained ~200 pN tension on syndecan-4 in cells treated with IgG1-κ isotype control antibody, or Anti-FN 3E3 Ab. Scale bar 20 μm, inset scale bar 5 μm. **d,** Mean active integrin β1 focal adhesion (FA) area. 13-36 cells were analysed with $n_{IgG1\text{-}κ\text{-}Control} = 274$, $n_{IgG1\text{-}κ\text{-}5min} = 407$, $n_{Anti\text{-}FN\text{-}Control} = 417$, $n_{Anti\text{-}FN\text{-}5min} = 203$ adhesions; two-sided Mann-Whitney test: $***P = 0.001$, n.s. $P = 0.581$. **e,** Total and active RhoA relative to unstimulated control for cells subjected to sustained syndecan-4 tension for 5-15 min in the presence of IgG1-κ and Anti-FN 3E3 antibodies. $n = 6$ biologically independent samples; general linear model for analysis of variance with Tukey pairwise comparisons: $***P =$

0.0006, *P = 0.0488, n.s. P ≥ 0.063. **f,** Representative phase contrast and wide field images for DNA, GFP, F-actin, and YAP in wild type (WT) and syndecan-4 null (Sdc4-/-) mouse embryonic fibroblasts on fibronectin. Scale bar 10 μm. **g,** Mean nuclear:cytoplasmic YAP intensity. n_{WT} = 43, $n_{Sdc4-/-}$ = 64, $n_{Sdc4-/-+WT-Sdc4-GFP}$ = 21 cells; general linear model for analysis of variance with Tukey pairwise comparisons: ***P < 0.001. **h,** Relative mRNA expression of YAP target genes connective tissue growth factor (*Ctgf*) and ankyrin repeat domain-1 (*Ankrd1*). n_{WT} = 5, $n_{Sdc4-/-}$ = 6 biologically independent samples; two-sided two-sample t-test: *P = 0.011, **P = 0.001. Boxes represent median and interquartile range, whiskers extend to the max/min data points; bar charts represent mean ± s.e.m.; individual values overlaid (a, e, h).

Figure 5. Syndecan-4 mechanotransduction requires the V-region which changes conformation under force. a, Schematic representation of syndecan-4 structure. **b,** Cytoplasmic domain amino acid sequences for wild type syndecan-4 (Sdc4WT), syndecan-4 which cannot be phosphorylated on Y180 (Sdc4Y180L), phospho-mimetic syndecan-4 (Sdc4Y180E), syndecan-4 truncated in the C2 domain (Sdc4Δ195E) and syndecan-4 truncated in the V domain (Sdc4Δ187I). **c,** Displacement of syndecan-4 bound beads in response to pulsatile 1 nN force in mouse embryonic fibroblast cell lines expressing wild type or mutant syndecan-4 on fibronectin, relative to force pulse 1. See Supplementary Fig. 15 for single cell data. n_{Sdc4WT} = 27, $n_{Sdc4Y180L}$ = 35, $n_{Sdc4Y180E}$ = 43, $n_{Sdc4Δ195E}$ = 23, $n_{Sdc4Δ187I}$ = 22 cells; Friedman test with Dunn pairwise comparisons: *P ≤ 0.0238, **P ≤ 0.0092, ***P ≤ 0.001 vs force pulse 1. Mean ± s.e.m. **d,** Molecular structure snapshots of syndecan-4 at 5 ns intervals during a 50 ns simulation with no force applied (molecular dynamics (MD)) and with constant force pulling at 50 pN on the extracellular domain of syndecan-4 (steered molecular dynamics (SMD)). **e-f,** Root mean square fluctuation (RMSF) of syndecan-4 Cα atoms overlaid on molecular structure (**e**) and plotted against residue (**f**). **g,** Average position of lysine K190 Cα atoms on the membrane plane representing directed movement of the cytoplasmic domain

from the virtual axis (located between transmembrane helices) towards the membrane in SMD. Average position was calculated for both K190 Cα atoms (chain A and B) in each 5 ns increment. See Supplementary Fig. 17 for amino acid sequence used in simulations.

Figure 6. Tension stabilises a syndecan-4/α-actinin/F-actin linkage to facilitate adaptive stiffening. a, Schematic representation of the interaction between syndecan-4 and α-actinin which provides a mechanical link to the cytoskeleton. α-actinin spectrin repeat 4 (SR4) binds to the syndecan-4 variable (V) domain, while the calponin-homology (CH) domains of α-actinin bind to F-actin. **b,** Representative wide field microscopy images of α-actinin-1 (ACTN1)-GFP expressing mouse embryonic fibroblasts (MEFs) pre (0 s) and post (60 s) the application of sustained tension on syndecan-4. MEFs were depleted of endogenous α-actinin-1 and α-actinin-4 (*siActn1Actn4*) and transfected to express ACTN1-GFP. Imaging conducted in the apical focal plane of the bead attachment. Scale bar: 20 μm. See Supplementary Fig. 20 for GFP control. **c,** Mean ACTN1-GFP intensity, in a region of interest surrounding the bead depicted by yellow dashed overlay, relative to mean intensity prior to force application. $n = 10$ cells; two-sided paired signed rank test: **$P = 0.002$. Boxes represent median and interquartile range, whiskers extend to the max/min data points, individual values are overlaid. **d,** Relative syndecan-4 bound bead displacement in MEFs treated with non-targeting control siRNA (siNT; $n = 18$) or siRNAs targeting *Actn1* and *Actn4* (si*Actn1Actn4*; $n = 18$) with expression of ACTN1-GFP (si*Actn1Actn4* + ACTN1-GFP; $n = 23$) or a mutant form of α-actinin with the actin binding domain (ABD) deleted (si*Actn1Actn4* + ACTN1-ΔABD-GFP; $n = 20$ cells). See Supplementary Fig. 21 for single cell data. Friedman test with Dunn pairwise comparisons: *$P \leq 0.0492$, **$P \leq 0.0058$, ***$P \leq 0.0009$ vs force pulse 1. Mean ± s.e.m. **e,** Schematic representation of the described mechanotransduction pathway where force on syndecan-4 (1) activates PI3K (2) in an EGFR-dependent manner. PIP₃ binds kindlin-2 leading to integrin

activation (3) and ligation of integrins with ECM which instigates RhoA signalling (4) leading to adaptive cell stiffening (5) with the potential to modulate matrix remodelling (6).
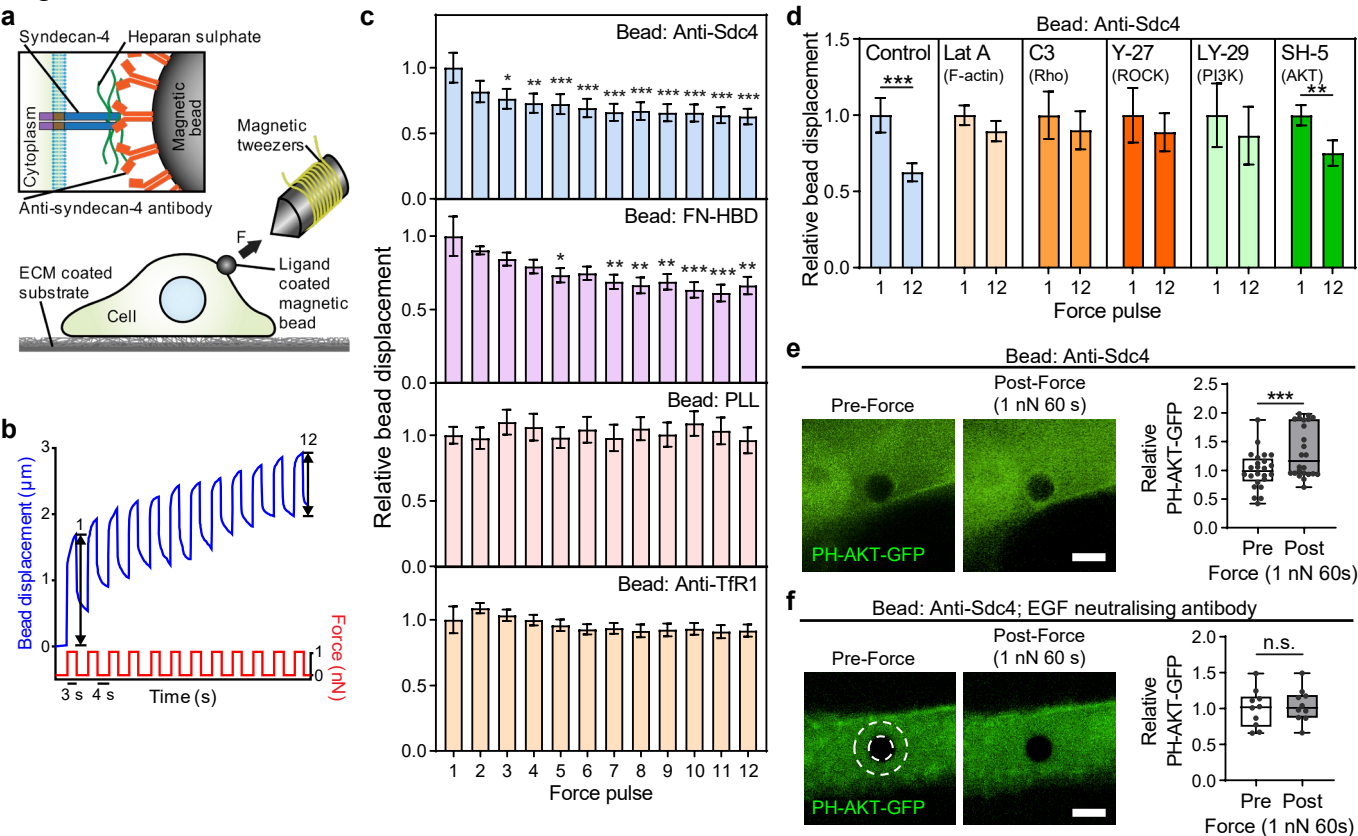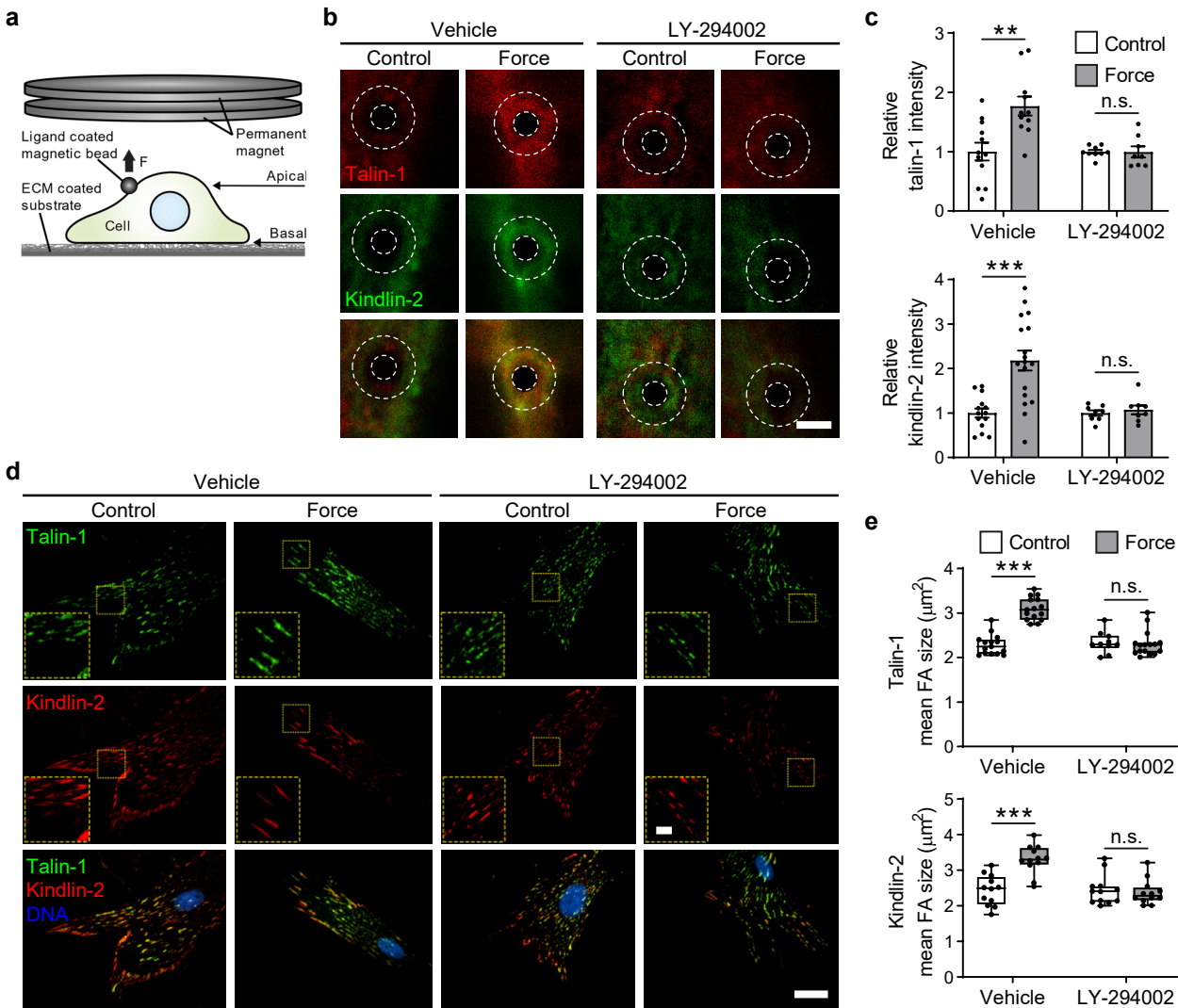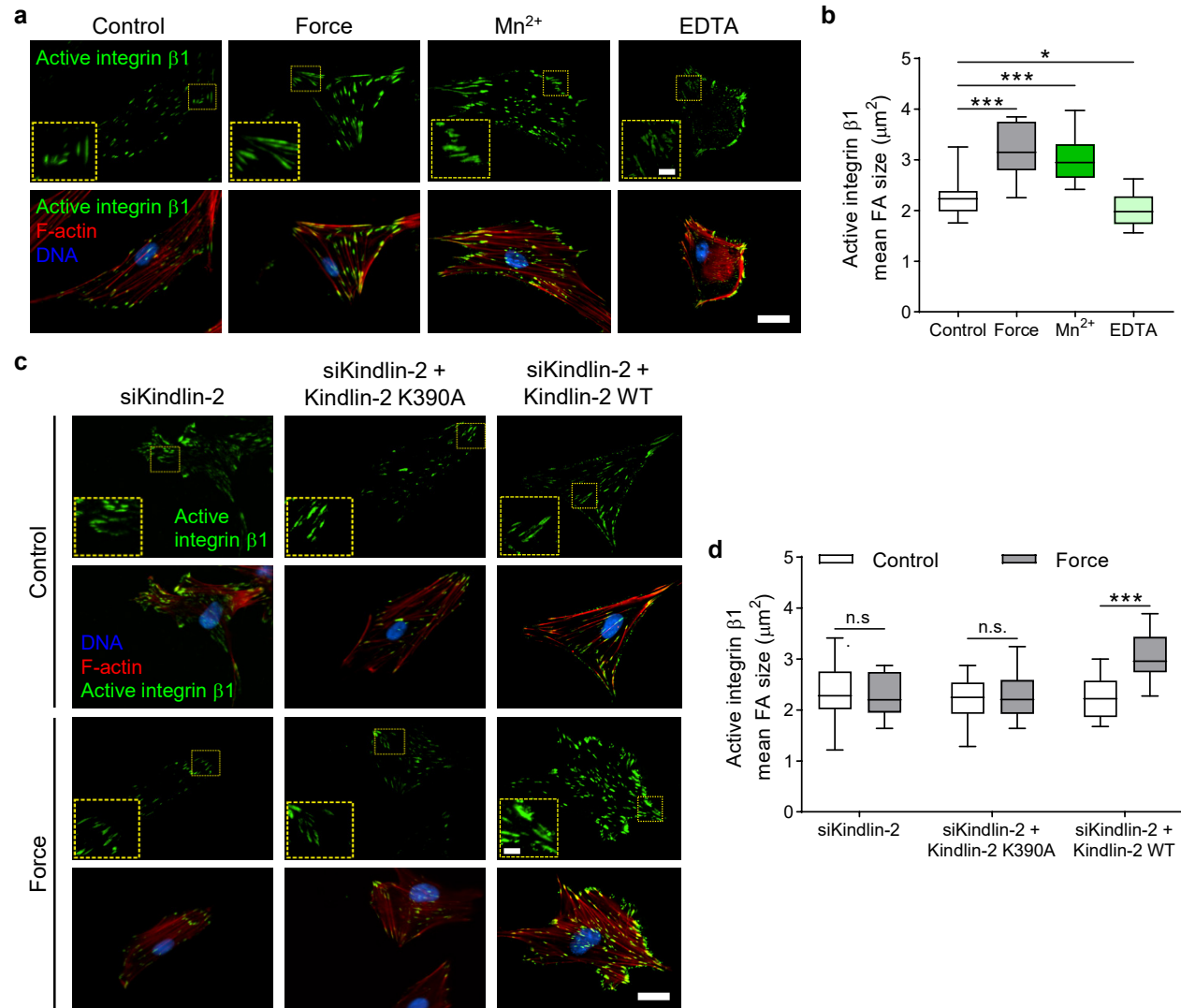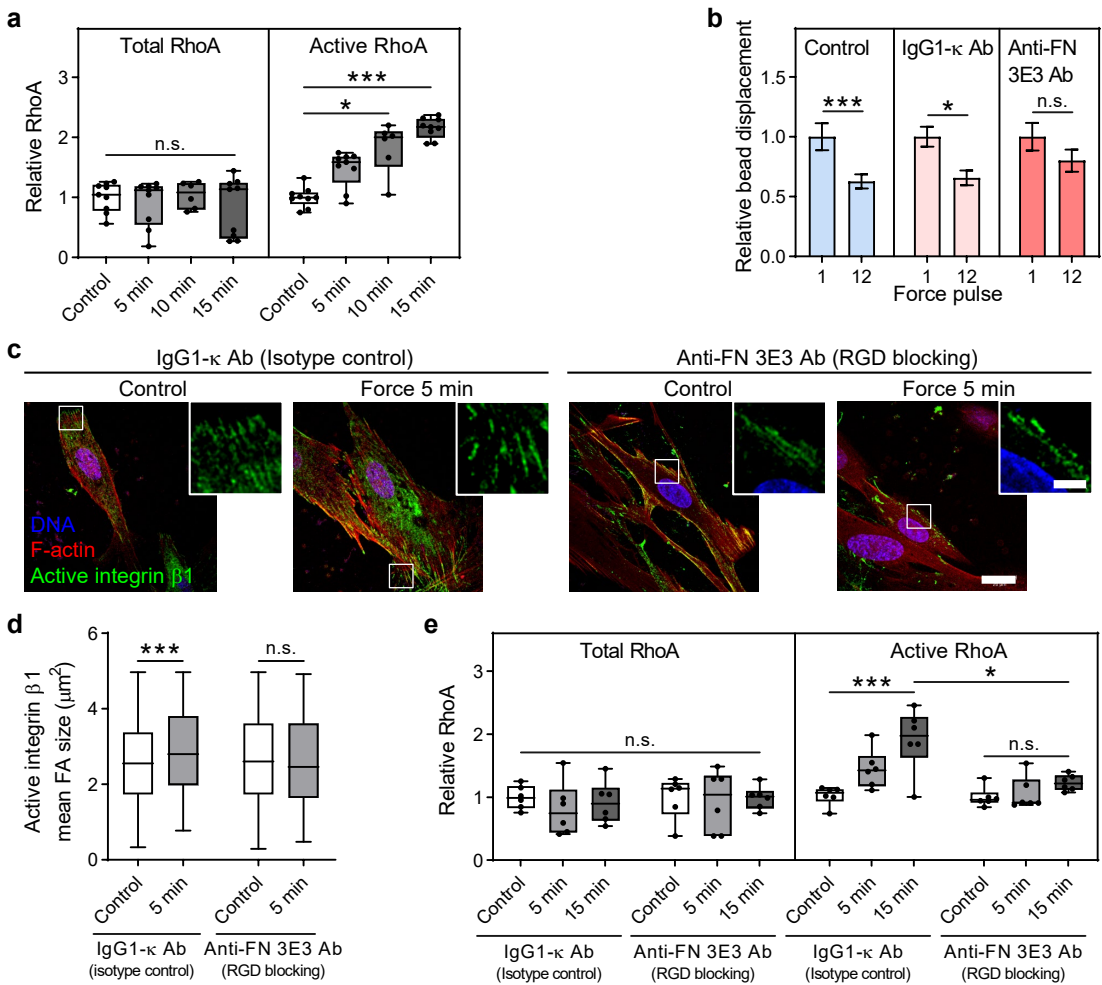
Figure 1

a

Syndecan-4
Heparan sulphate
Magnetic bead
Cytoplasm
Anti-syndecan-4 antibody
Magnetic tweezers
F
Ligand coated magnetic bead
ECM coated substrate
Cell

b Bead displacement (μm) / Force (nN)
1
12
3 s 4 s
Time (s)

c Relative bead displacement / Force pulse
Bead: Anti-Sdc4
* ** *** *** *** *** *** *** *** *** ***
Bead: FN-HBD
* ** ** ** *** *** **
Bead: PLL
Bead: Anti-TfR1
1 2 3 4 5 6 7 8 9 10 11 12

d Relative bead displacement
Bead: Anti-Sdc4
Control | Lat A (F-actin) | C3 (Rho) | Y-27 (ROCK) | LY-29 (PI3K) | SH-5 (AKT)
*** **
1 12
Force pulse

e Bead: Anti-Sdc4
Pre-Force | Post-Force (1 nN 60 s)
PH-AKT-GFP
Relative PH-AKT-GFP
***
Pre Post
Force (1 nN 60s)

f Bead: Anti-Sdc4; EGF neutralising antibody
Pre-Force | Post-Force (1 nN 60 s)
PH-AKT-GFP
Relative PH-AKT-GFP
n.s.
Pre Post
Force (1 nN 60s)

Figure 2

a Ligand coated magnetic bead, Permanent magnet, F, Apical, ECM coated substrate, Cell, Basal

b Vehicle / LY-294002 — Control, Force, Control, Force — Talin-1, Kindlin-2

c Relative talin-1 intensity / Relative kindlin-2 intensity — Control, Force — Vehicle, LY-294002; ** , n.s., *** , n.s.

d Vehicle / LY-294002 — Control, Force, Control, Force — Talin-1, Kindlin-2, Talin-1 Kindlin-2 DNA

e Talin-1 mean FA size (µm²) / Kindlin-2 mean FA size (µm²) — Control, Force — Vehicle, LY-294002; *** , n.s., *** , n.s.

Figure 3

Figure 4

―― RhoA mediated stiffening requires β1 integrin ligation ――

a

b

c

IgG1-κ Ab (Isotype control)   Anti-FN 3E3 Ab (RGD blocking)

d   **e**

―― Syndecan-4 mechanosignalling is required for YAP activation ――

f   WT   Sdc4-/-   Sdc4-/- + WT-Sdc4-GFP

g   **h**

Figure 5

Figure 6

a

Variable domain · Conserved domains · Syndecan-4 · α-Actinin · F-actin · Plasma membrane · Extracellular · Cytoplasmic · C1 V C2 · SR4 SR3 SR2 SR1 · CH1 CH2

b

Pre-Force · Post-Force (1 nN 60 s) · ACTN1-GFP · si*Actn1Actn4* + ACTN1-GFP

c

Relative ACTN1-GFP intensity · Pre · Post · Force (1 nN 60s) · **

d

Relative bead displacement · Force pulse

siNT · si*Actn1Actn4* + ACTN1-GFP · si*Actn1Actn4* · si*Actn1Actn4* + ACTN1-ΔABD-GFP

e

(1) Force · PIP$_3$ · EGFR · Plasma membrane · Nucleus · YAP · Syndecan-4 dimer · (2) PI3K · α-actinin · F-actin · (4) RhoA · (5) Adaptive cell stiffening · (3) Integrin activation · Kindlin-2 · Integrins · Extracellular matrix · (6) Cell mediated matrix remodelling?

Syndecan-4 tunes cell mechanics by activating the kindlin-integrin-RhoA pathway

Antonios Chronopoulos[1][†], Stephen D. Thorpe[2][†][*], Ernesto Cortes[1], Dariusz Lachowski[1], Alistair J. Rice[1], Vasyl V. Mykuliak[3,4], Tomasz Róg[5], David A. Lee[2], Vesa P. Hytönen[3,4][*], Armando E. del Río Hernández[1][*]

[1]Cellular and Molecular Biomechanics Laboratory, Department of Bioengineering, Imperial College London, London, United Kingdom

[2]Institute of Bioengineering, School of Engineering and Materials Science, Queen Mary University of London, London, United Kingdom

[3]Faculty of Medicine and Health Technology and BioMediTech, Tampere University, Tampere, Finland

[4]Fimlab Laboratories, Tampere, Finland

[5]Department of Physics, University of Helsinki, Helsinki, Finland

[†]These authors contributed equally: Antonios Chronopoulos, Stephen D. Thorpe.

[*]Correspondence should be addressed to A.E.d.R.H. (a.del-rio-hernandez@imperial.ac.uk), V.P.H. (vesa.hytonen@tuni.fi) or S.D.T. (s.thorpe@qmul.ac.uk).

Supplementary Information
- Supplementary Figures
- Supplementary Discussion
- Supplementary Methods
- Supplementary References

Supplementary Figures
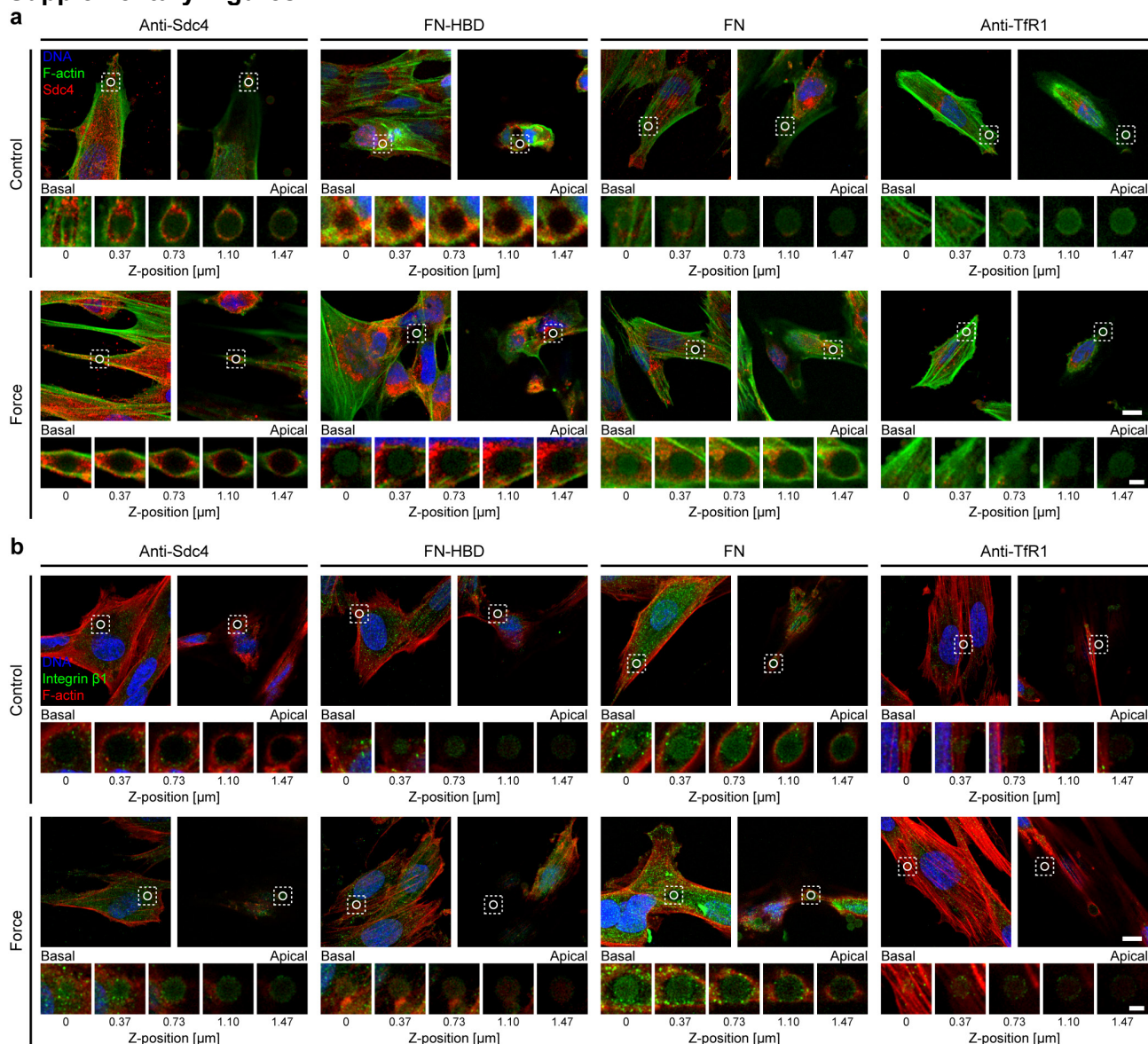
Supplementary Figure 1: Specificity of functionalised bead binding to syndecan-4. a,b,
Immunofluorescent staining for (**a**) syndecan-4 (Sdc4) and (**b**) integrin β1 with f-actin and DNA as indicated. Representative basal and apical confocal z-sections are presented with higher magnification insets of the bead attachment region at a z-section spacing of 0.366 μm. To assess the specificity of cell binding to functionalised beads, pancreatic stellate cells were plated on fibronectin coated coverslips and beads allowed to attach for 30 min. Beads were functionalised with mouse anti-syndecan-4 (Anti-Sdc4) ectodomain antibody, the heparin binding domain fragment of fibronectin (FN-HBD), unmodified fibronectin (FN), and mouse anti-transferrin receptor protein-1 (Anti-TfR1). Unbound beads were removed with a PBS wash. A permanent magnet was used to apply a sustained force of approx. 200 pN to cell-bound beads for 5 min. Cells were fixed immediately post force application, and immunofluorescently stained followed by confocal imaging of bead attachment sites. Note the presence of intense syndecan-4 (red) staining in the bead attachment region in beads functionalised with anti-Sdc4, FN-HBD and FN, and the absence of this in anti-TfR1 beads in (**a**). Similarly note the absence of integrin β1 (green) surrounding beads in control (unstimulated) anti-Sdc4, FN-HBD and Anti-TfR1 beads in (**b**). Force led to accumulation of Sdc4 and/or integrin β1 at the bead site for anti-Sdc4, FN-HBD and FN beads, while no increase was evident for anti-TfR1 beads which do not elicit a mechanoresponse. Experiments were repeated independently twice with consistent results. Full field scale bar 10 μm; inset scale bar 2.5 μm.
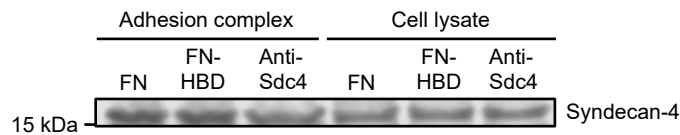
Supplementary Figure 2: Western blot confirming syndecan-4 (Sdc4) binding to functionalised cell-bound beads. Syndecan-4 is present in the adhesion complex with fibronectin (FN), 40K Heparin binding domain of fibronectin (FN-HBD), and anti-syndecan-4 antibody (Anti-Sdc4) coated beads. Functionalised beads were allowed attach to pancreatic stellate cells for 30 min before cell lysis and magnetic isolation of the bead bound adhesion complex. Representative blot from three independent experiments with similar results.
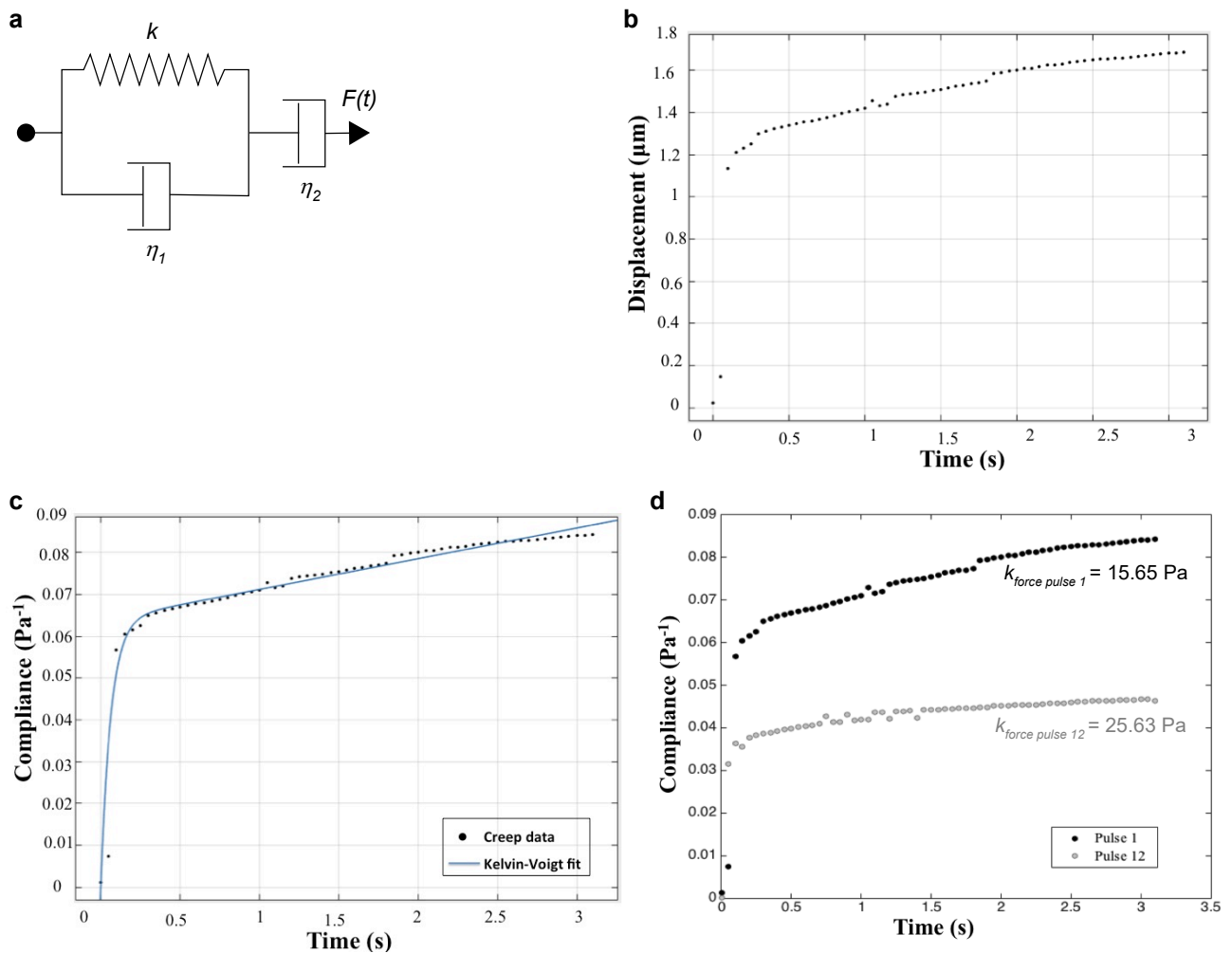
Supplementary Figure 3: Tension on syndecan-4 increases cellular stiffness. To examine the cell stiffness in response to an applied force, the time-dependent compliance ($J(t)$) of the cell was calculated from the time-dependent bead displacement ($x(t)$) using $J(t)=6\pi ax(t)/F(t)$, where a is the bead radius. The viscoelastic response of the cell was characterized by fitting the creep compliance during force application to a modified Kelvin-Voigt model used to describe viscoelastic materials. **a,** Schematic representation of the modified Kelvin-Voigt model comprising a spring and dashpot in parallel, with a dashpot in series. **b,** Representative bead displacement curve for first force pulse. **c,** Representative bead displacement curve transformed into compliance and fitted to the modified Kelvin-Voigt model. **d,** Comparison of cell stiffness denoted by the spring constant k during the first and last 1 nN force pulse. Representative cell stiffness matches data presented in Figure 1b from n = 32 cells.
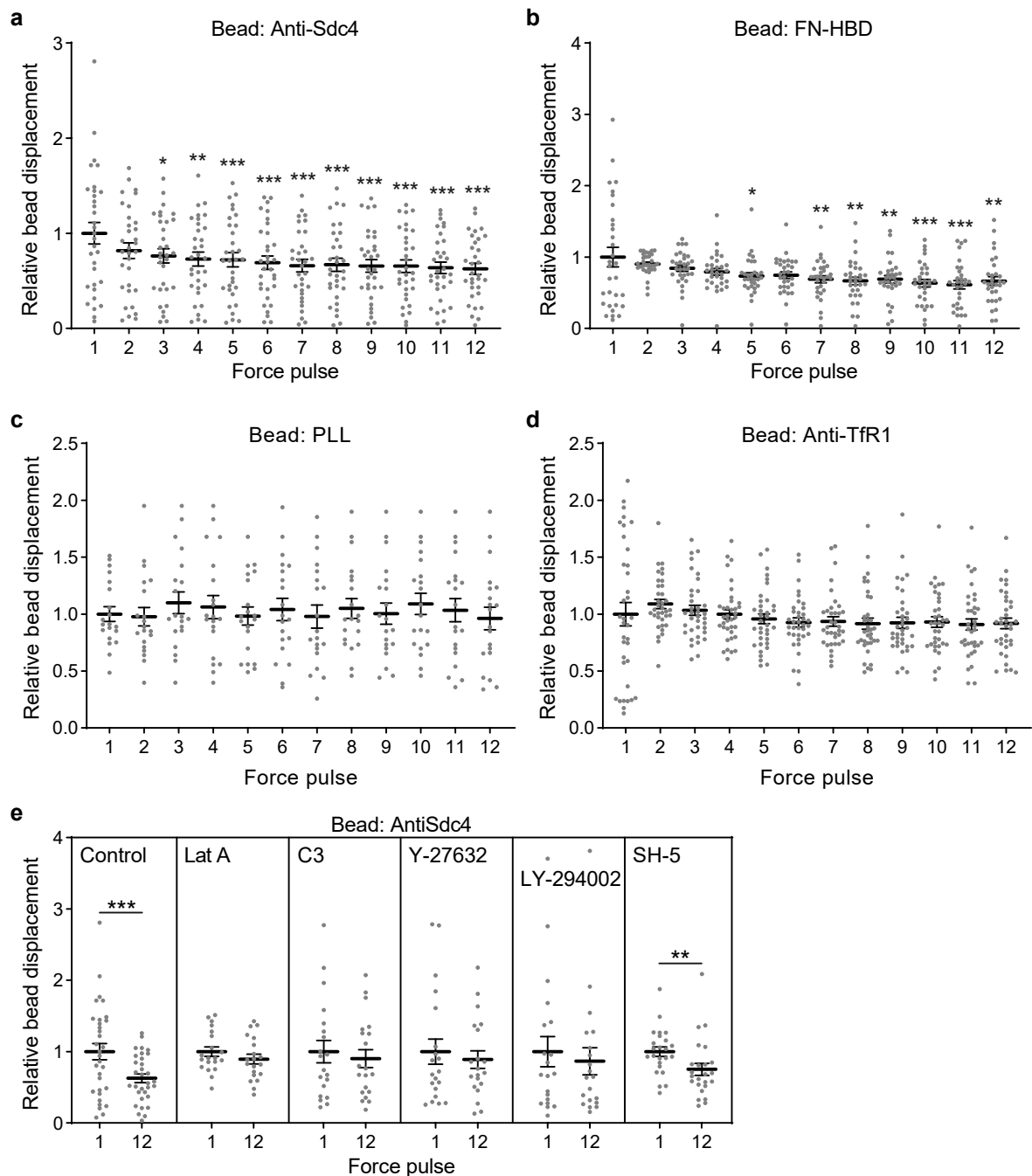
Supplementary Figure 4: Single cell data corresponding to summarised magnetic tweezers bead displacement data presented in Figure 1. Magnetic bead displacement amplitude in response to a 1 nN pulsatile force is presented for each pancreatic stellate cell (PSC) relative to the average first pulse displacement. **a-d,** Beads were functionalised with (**a**) mouse anti-syndecan-4 ectodomain antibody (Anti-Sdc4; *n* = 32), (**b**) the heparin binding domain fragment of fibronectin (FN-HBD; *n* = 31), (**c**) poly-L-lysine (PLL; *n* = 20), and (**d**) mouse anti-transferrin receptor protein-1 (Anti-TfR1; *n* = 36 cells). Friedman test with Dunn pairwise comparisons: *$*P \leq$ 0.0116, $**P \leq 0.0041$, $***P < 0.0001$ vs force pulse 1. **e,** Single cell data for relative magnetic bead displacement at force pulse 1 and 12 for Anti-Sdc4 magnetic beads bound to untreated control PSCs (*n* = 32) or PSCs treated with F-actin polymerisation inhibitor latrunculin A (Lat A; 0.5 μM, 1 h; *n* = 20), Rho inhibitor C3 transferase (C3; 2 μg/mL, 4 h; *n* = 20), Rho-associated protein kinase (ROCK) inhibitor Y-27632 (10 μM, 1 h, *n* = 20), phosphoinositide 3-kinase (PI3K) inhibitor LY-294002 (30 μM, 1 h; *n* = 20), or AKT inhibitor SH-5 (10 μM, 1 h; *n* = 24 cells). Two-sided paired signed rank test: $**P = 0.002$, $***P < 0.0001$. Grey dots represent individual bead displacements, mean and s.e.m. overlaid.

4
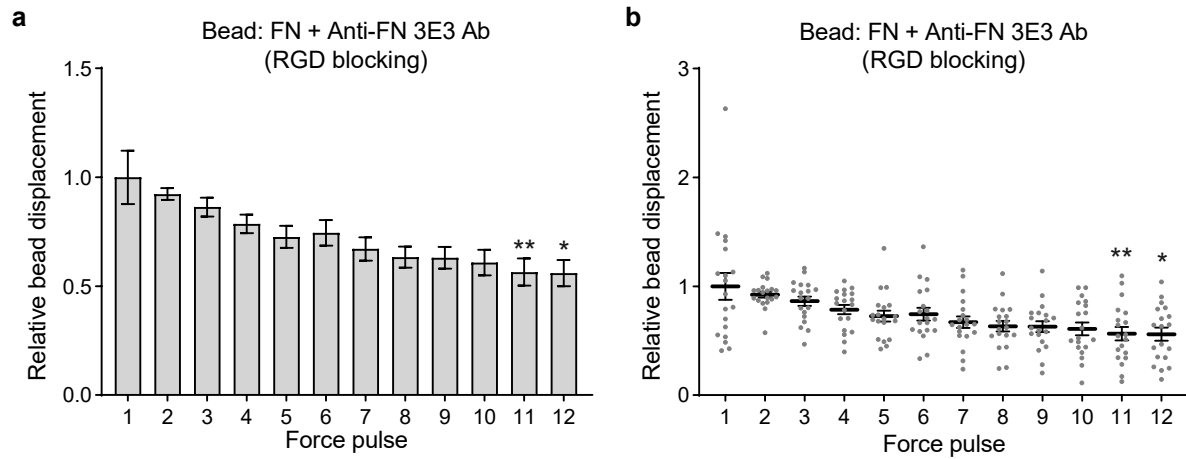
Supplementary Figure 5: Force applied to syndecan heparan sulphate chains induces adaptive cell stiffening. a,b, Magnetic bead displacement amplitude in response to a 1 nN pulsatile force is presented as summarised mean value (**a**) and for each pancreatic stellate cell (**b**) relative to the average first pulse displacement. Beads were functionalised with fibronectin treated with an RGD integrin binding site blocking antibody (clone 3E3) which leaves the heparin binding domain available (FN + Anti-FN 3E3 Ab; n = 19 cells). Friedman test with Dunn pairwise comparisons: *P = 0.0104, **P = 0.0054 vs force pulse 1. Mean ± s.e.m. with individual values overlaid.
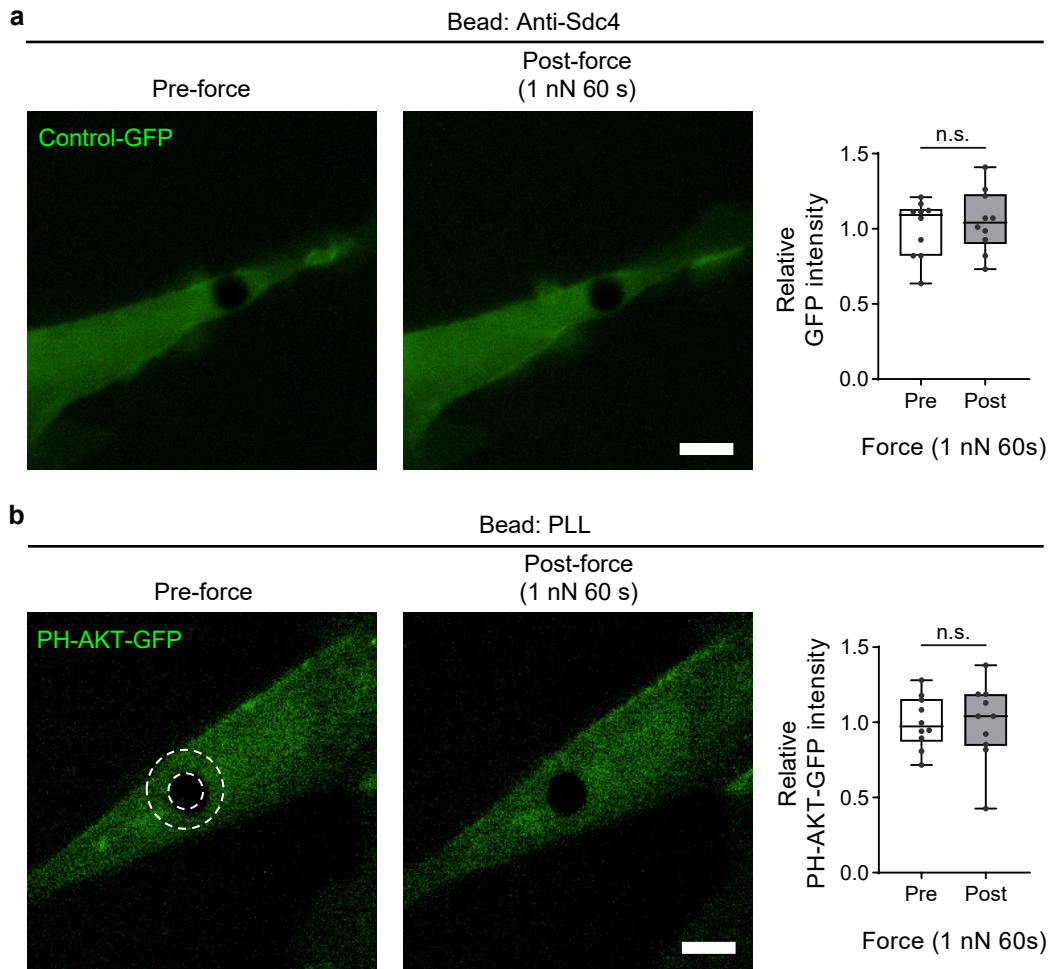
Supplementary Figure 6: Confirmation of specificity of force induced PI3K activation to syndecan-4. a, Sustained force applied to syndecan-4 bound beads on pancreatic stellate cells expressing an empty control GFP vector did not lead to GFP accumulation in the bead region, unlike in cells expressing the PIP$_3$ biosensor PH-AKT-GFP (Fig. 1e). **b,** Sustained force applied to poly-L-lysine (PLL) coated beads attached to cells expressing PH-AKT-GFP did not lead to PH-AKT-GFP accumulation at the bead; indicating that force-induced PI3K activation is specific to syndecan-4. Cells expressing either vector were exposed to a sustained tensional force of 1 nN for 60 s. Representative images of the area surrounding the magnetic bead pre (0 s) and post (60 s) force application. Mean PH-AKT-GFP fluorescent intensity, in a region of interest surrounding the bead depicted by white dashed overlay, is presented relative to mean intensity prior to force application. Scale bar: 5 μm. n = 10 cells from 2 biologically independent experiments; two-sided paired signed rank test: (a) n.s. P = 0.655, (b) n.s. P = 0.987. Boxes represent median and interquartile range, whiskers extend to the max/min data points, individual values are overlaid.
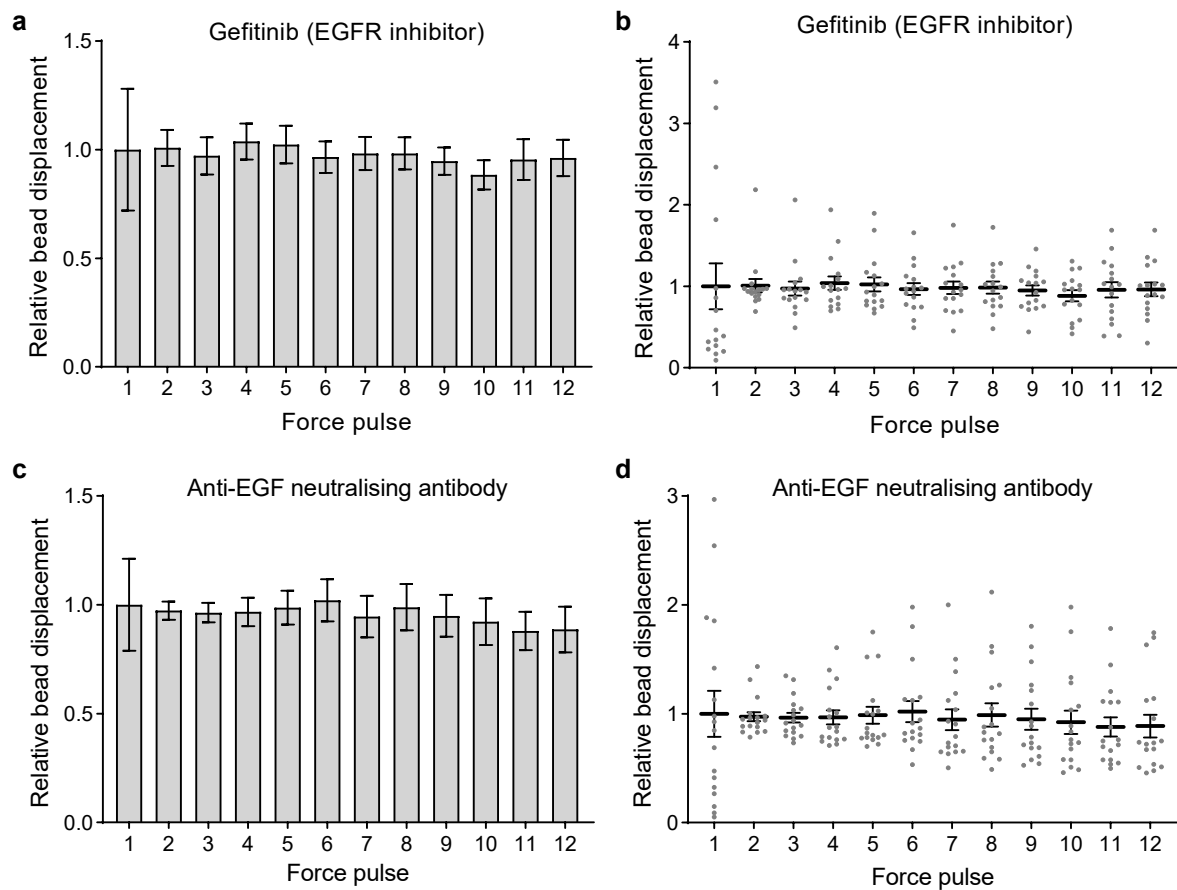
Supplementary Figure 7: EGFR is required for syndecan-4 mediated adaptive cell stiffening. Pulsatile force applied to syndecan-4 bound beads in the presence of **a,b,** Epidermal growth factor receptor (EGFR) inhibitor Gefitinib (Santa Cruz Biotechnology sc-202166, 15 μM, 2h; *n* = 16 cells) or **c,d**, anti-epidermal growth factor (EGF) neutralising antibody (R&D Systems MAB236, 5 μg ml^{-1}, 30 min; *n* = 17 cells) did not induce an adaptive stiffening response. Magnetic bead displacement amplitude in response to a 1 nN pulsatile force is presented as mean (**a**,**c**) and for each pancreatic stellate cell (**b**,**d**) relative to the average first pulse displacement. Beads were functionalised with mouse anti-syndecan-4 ectodomain antibody. Mean ± s.e.m. with individual values overlaid.
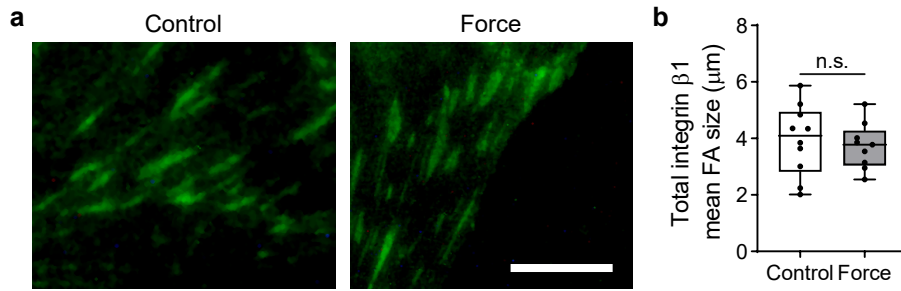
Supplementary Figure 8: Total integrin β1 incorporation into focal adhesions does not change in response to tension on syndecan-4. a, Representative epifluorescent microscopy images of total integrin β1 at the basal surface of pancreatic stellate cells in control conditions or in response to a sustained tensional force of approx. 200 pN for 5 min applied using a permanent magnet. Cells were fixed immediately post force application and immunofluorescently stained for integrin β1. Scale bar 5 μm. **b,** Quantification of mean focal adhesion size for integrin β1 containing adhesions. The mean adhesion size from > 10 focal adhesions from 3 regions of interest per cell are presented. $n_{Control}$ = 10 cells, n_{Force} = 9 cells; two-sided two-sample t-test: n.s. P = 0.678. Boxes represent median and interquartile range, whiskers extend to the max/min data points, with mean cell values overlaid.
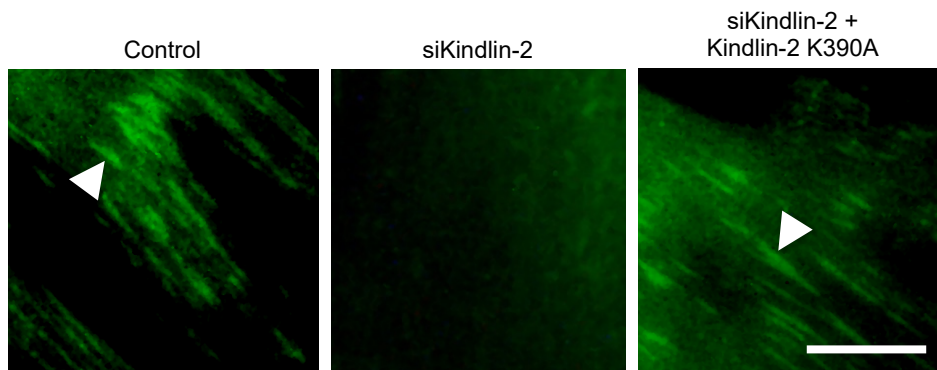
Supplementary Figure 9: Immunofluorescent staining demonstrating knockdown and re-expression of kindlin-2. Representative epifluorescent microscopy images of kindlin-2 at the basal surface of pancreatic stellate cells. Cells were left untreated (Control), treated with siRNA targeting kindlin-2 (siKindlin-2), and subsequently transfected with a plasmid to re-express a kindlin-2 mutant (K390A) lacking phosphoinositide binding activity (siKindlin-2 + Kindlin-2 K390A). Cells were fixed and immunofluorescently stained for kindlin-2. White arrowheads indicate incorporation of kindlin-2 in focal adhesions with no kindlin-2 positive adhesions observed in the siKindlin-2 condition. Representative images from 2 independent repeat experiments. Scale bar 5 μm.
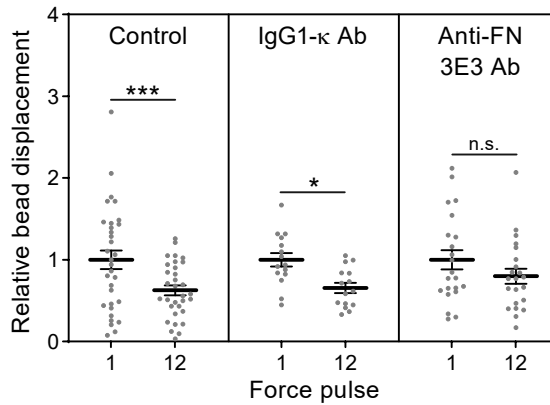
Supplementary Figure 10: Single cell data corresponding to summarised magnetic tweezers bead displacement data presented in Figure 4b. Bead displacement presented relative to the mean value for force pulse 1. Pulsatile force applied to syndecan-4 bound beads on pancreatic stellate cells plated on fibronectin in untreated control conditions (n = 32), in the presence of isotype control mouse IgG1-κ antibody (clone MOPC-21, Merck MABF1081Z; n = 15), and in the presence of mouse anti-fibronectin antibody (clone 3E3, Merck MAB88916-C), which blocks the RGD integrin binding site of fibronectin preventing new integrin-RGD connections (n = 22 cells). Both antibodies were added at 20 μg ml^{-1} for 30 min prior to initiation of magnetic tweezer stimulation and were maintained throughout experiments. Two-sided paired signed rank test: *P = 0.035, ***P < 0.0001, n.s. P = 0.134. Mean $\pm$ s.e.m. with individual values overlaid.
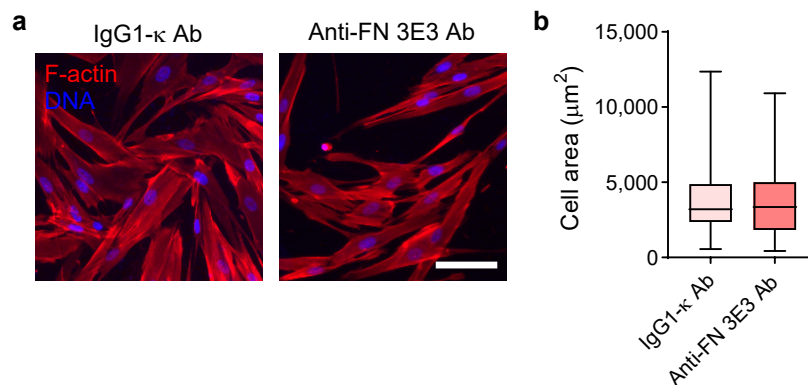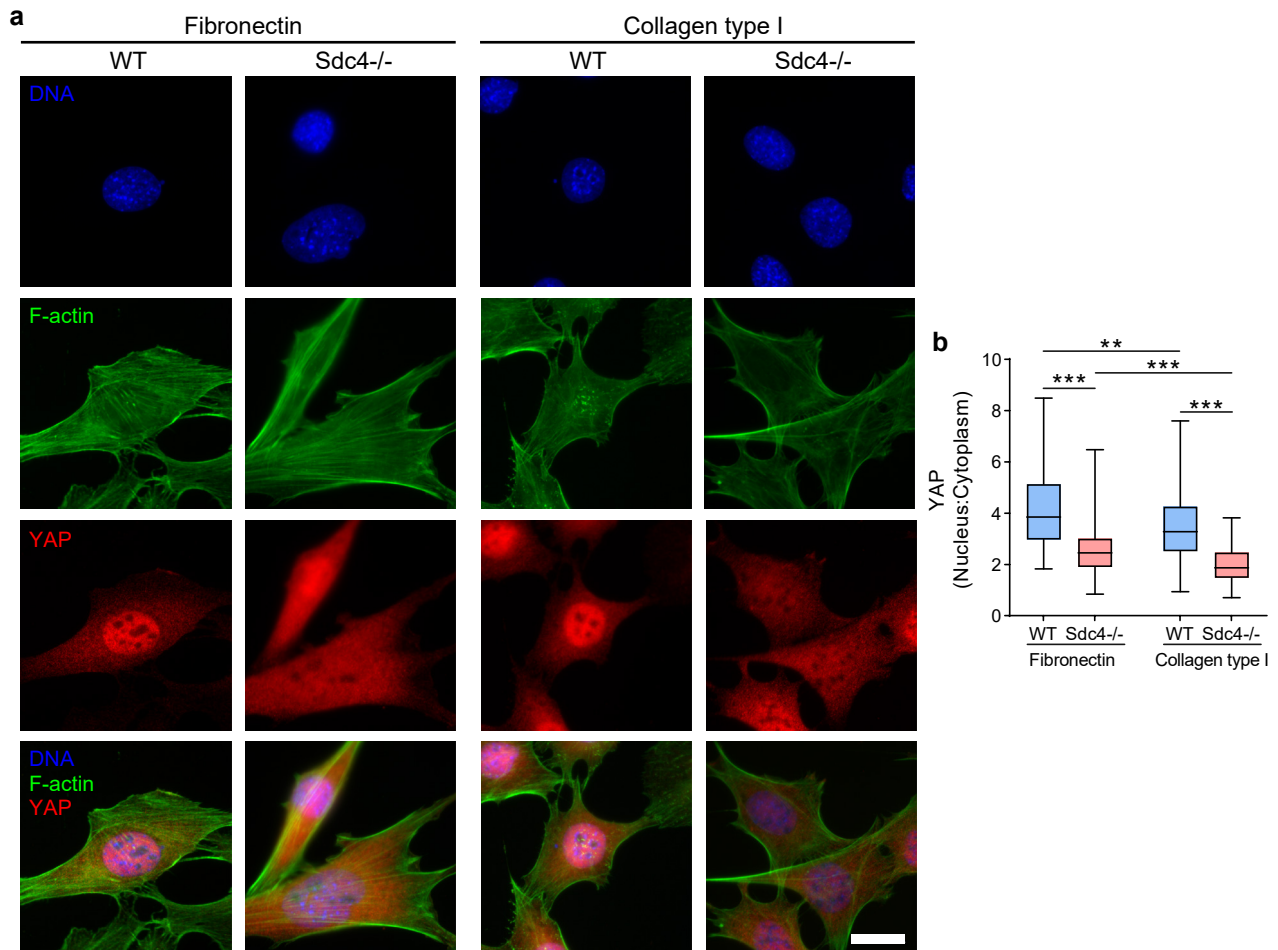

Supplementary Figure 11: Blocking of fibronectin's RGD binding site does not alter cell spread area. a, Representative epifluorescent microscopy images of f-actin in pancreatic stellate cells in the presence of isotype control mouse IgG1-κ antibody (clone MOPC-21, Merck MABF1081Z) or mouse anti-fibronectin antibody (clone 3E3, Merck MAB88916-C), which blocks the RGD integrin binding site of fibronectin preventing new integrin-RGD connections. Both antibodies were added at 20 μg ml^{-1} for 30 min prior to fixation of cells. Scale bar 100 μm. **b,** Quantification of cell spread area corresponding to images in (**a**). Morphological outlines were manually traced on F-actin overlays in ImageJ. $n_{IgG1-\kappa}$ = 142 cells, $n_{Anti-FN\ 3E3}$ = 91 cells; two-sided Mann-Whitney test: P = 0.416. Boxes represent median and interquartile range, whiskers extend to the max/min data points.
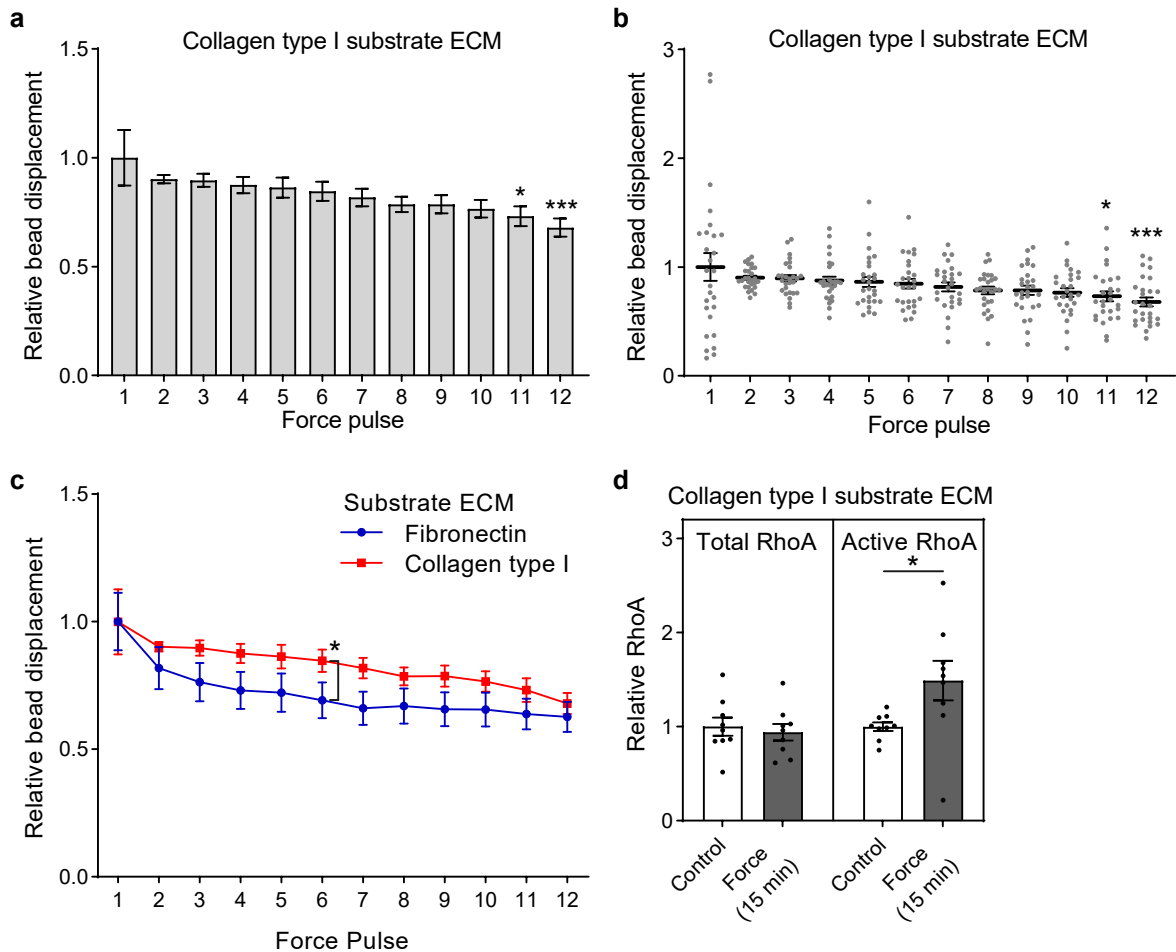
Supplementary Figure 12: Syndecan-4 tension mediated cell stiffening and RhoA activation persists in cells seeded on collagen type I. a,b, 1 nN pulsatile force was applied to syndecan-4 bound beads on pancreatic stellate cells (PSCs) plated on collagen type I. Mean (**a**) and individual cell (**b**) bead displacement presented relative to the average displacement of force pulse 1. n = 27 cells; Friedman test with Dunn pairwise comparisons: *P = 0.0179, ***P = 0.0007 vs force pulse 1. **c,** Relative syndecan-4 bound bead displacement for PSCs plated on fibronectin (n = 32, see Supplementary Fig. 3) and on collagen as presented in (**a**,**b**). The reduction in bead displacement with each force pulse is less rapid in cells on collagen compared to cells on fibronectin. $n_{Fibronectin}$ = 32, $n_{Collagen\ type\ I}$ = 27 cells; two-sided two sample t-test: *P = 0.046. **d,** Syndecan-4 bound beads on PSCs plated on collagen type I were subjected to sustained tension of ~200 pN for 15 min, with total and active RhoA assessed using ELISA and G-LISA respectively, presented relative to unstimulated control. The application of sustained force led to an increase in RhoA activation, but this was less marked as that in cells on fibronectin (Fig. 4a). n = 9 biologically independent samples; two-sided two-sample t-test: *P = 0.037. Mean ± s.e.m. with individual values overlaid.
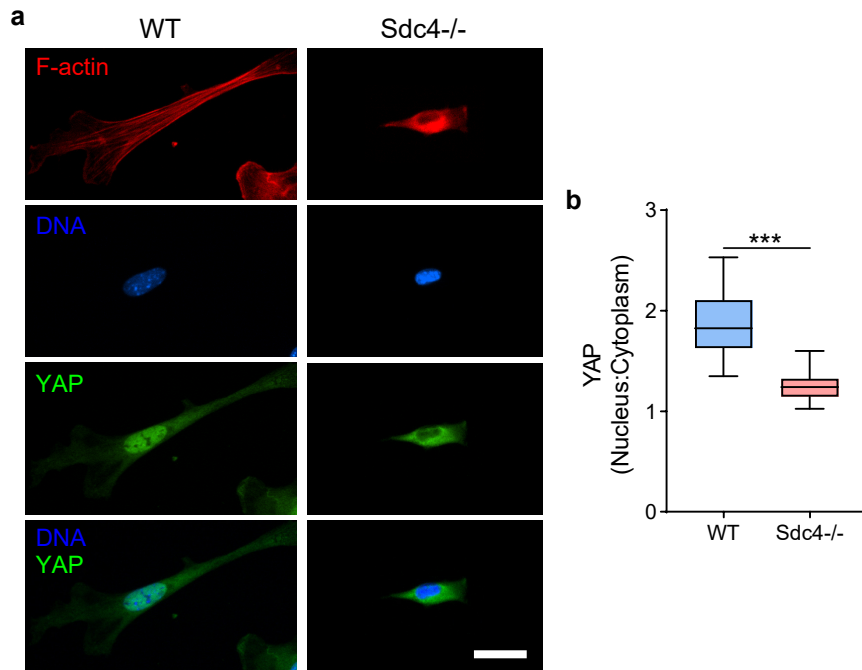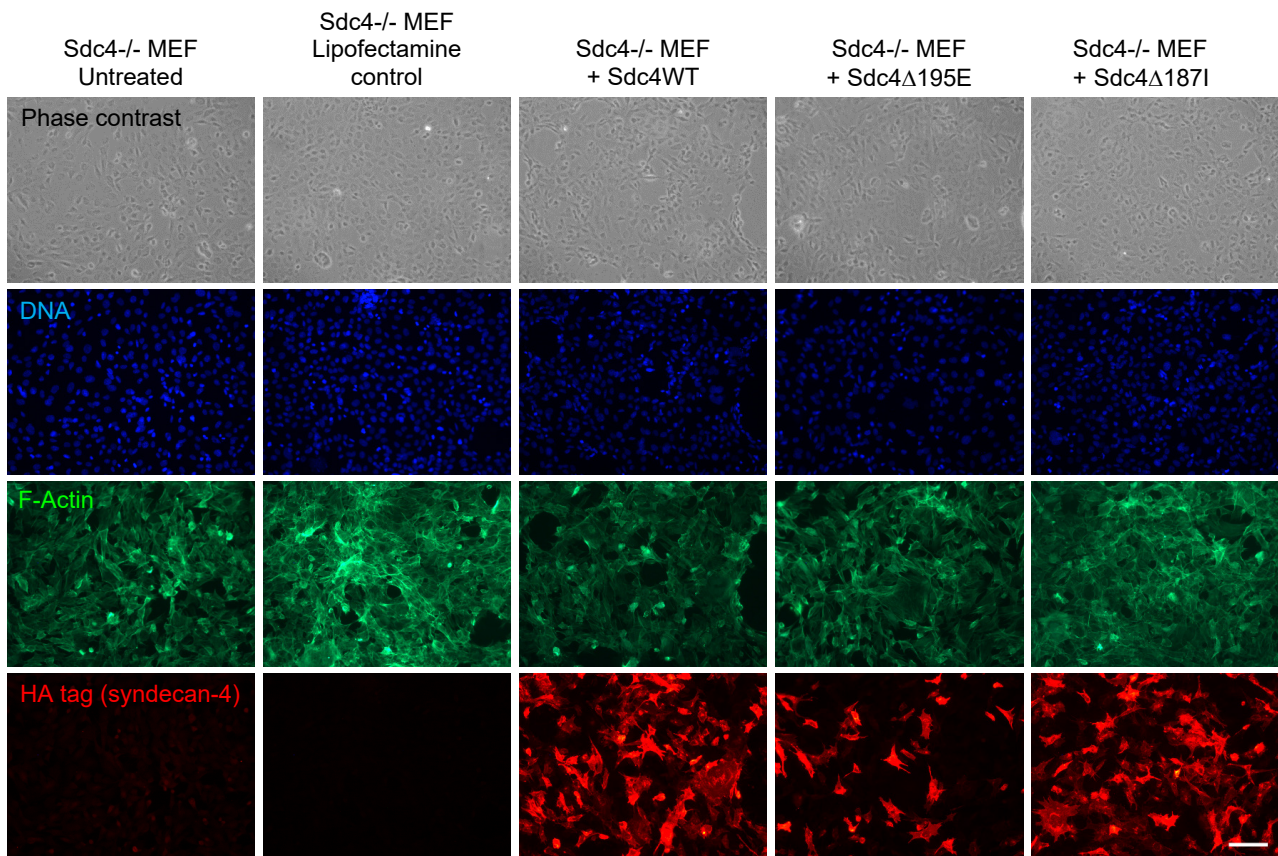
Supplementary Figure 13. Syndecan-4 is required for YAP nuclear localisation on fibronectin coated 25 kPa gels. a, Wild type (WT) and syndecan-4 null (Sdc4-/-) mouse embryonic fibroblasts were plated onto fibronectin coated 25 kPa polyacrylamide gels, fixed and immunofluorescently stained for YAP. Representative wide field microscopy images for DNA, F-actin and YAP. Scale bar 20 μm. **b,** Quantification of mean nuclear:cytoplasmic YAP intensity. n_{WT} = 18, $n_{Sdc4-/-}$ = 16 cells; two-sided two-sample t-test: ***P < 0.0001. Boxes represent median and interquartile range, whiskers extend to the max/min data points.

Supplementary Figure 14: Syndecan-4 is required for YAP nuclear translocation in mouse embryonic fibroblasts plated on fibronectin or collagen type I. Wild type (WT) and syndecan-4 null (Sdc4-/-) mouse embryonic fibroblasts were plated on fibronectin or collagen type I coated substrates. **a,** Representative epifluorescent microscopy images for DNA, F-actin, YAP and merged channels. Scale bar 20 μm. **b,** Quantification of mean nuclear:cytoplasmic YAP intensity. $n_{Fibronectin-WT}$ = 96, $n_{Fibronectin-Sdc4-/-}$ = 82, $n_{Collagen\ 1-WT}$ = 91, $n_{Collagen\ 1-Sdc4-/-}$ = 172 cells; two-sided Mann-Whitney tests: **P = 0.005, ***P < 0.001. Boxes represent median and interquartile range, whiskers extend to the max/min data points. YAP downregulation in Sdc4-/- cells was not affected by substrate ECM with Sdc4-/- cells on collagen type I exhibiting a reduction in nuclear YAP compared to WT. Both WT and Sdc4-/- cells exhibited decreased nuclear:cytoplasmic YAP on collagen type I compared to fibronectin.
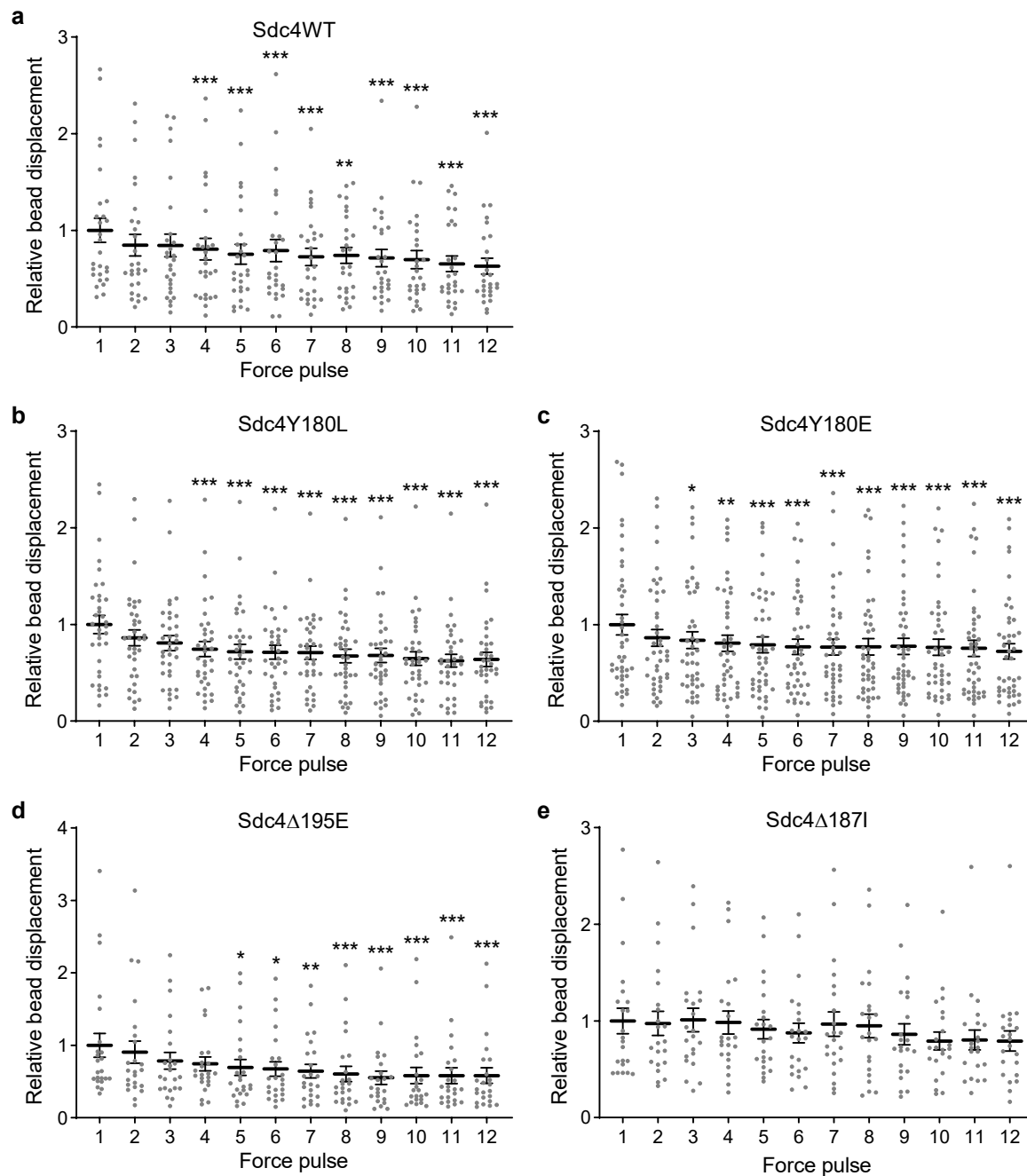
Supplementary Figure 15: Single cell data corresponding to summarised magnetic tweezers bead displacement data presented in Figure 5c. a-e, Bead displacement presented relative to the mean value for force pulse 1 in response to 1 nN pulsatile force applied to syndecan-4 bound beads on mouse embryonic fibroblasts (MEFs) plated on fibronectin. MEF cell lines expressing (**a**) wild type syndecan-4 (Sdc4WT; n = 27), (**b**) phospho-null syndecan-4 (Sdc4Y180L; n = 35), (**c**) phospho-mimetic syndecan-4 (Sdc4Y180E; n = 43), (**d**) syndecan-4 truncated in the C2 domain (Sdc4Δ195E; n = 23), or (**e**) syndecan-4 truncated in the variable (V) domain (Sdc4Δ187I; n = 22 cells). Friedman test with Dunn pairwise comparisons: *$P \leq 0.0238$, **$P \leq 0.0092$, ***$P \leq 0.001$ vs force pulse 1. Mean ± s.e.m. with individual values overlaid.

Supplementary Figure 16: Confirmation of syndecan-4 plasmid transfection into syndecan-4 null (Sdc4-/-) mouse embryonic fibroblast (MEF) line. Representative epifluorescent microscopy images of immunofluorescent staining for F-actin and HA tagged syndecan-4 plasmid expression. Sdc4-/- MEFs expressing wild type syndecan-4 (Sdc4WT), syndecan-4 truncated in the C2 domain (Sdc4Δ195E), or syndecan-4 truncated in the variable domain (Sdc4Δ187I) were fixed 24 h post transfection. Images are representative from 2 biologically independent experiments with similar results. Scale bar 100 μm.

a

```
MAPARLFALL LFFVGGVAES IRETEVIDPQ DLLEGRYFSG 40
ALPDDEDVVG PGQESDDFEL SGSGDLDDLE DSMIGPEVVH 80
PLVPLDNHIP ERAGSGSQVP TEPKKLEENE VIPKRISPVE 120
ESEDVSNKVS MSSTVQGSNI FERTEVLAAL IVGGIVGILF 160
AVFLILLLMY RMKKKDEGSY DLGKKPIYKK APTNEFYA 198
```

C1 region Variable region C2 region

Signal peptide
Extracellular domain
Transmembrane domain
Cytoplasmic domain (C1, Variable and C2 regions)
Sequence included in the simulations

b

50 pN

replica 1 replica 2 replica 3 replica 4
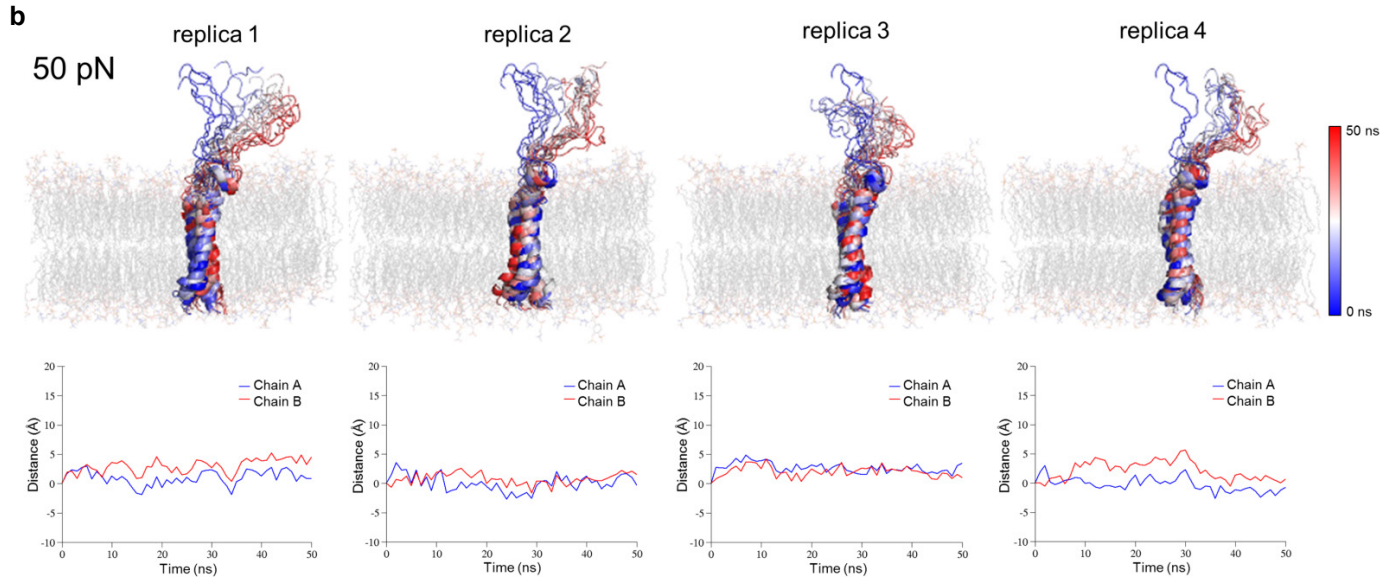
Supplementary Figure 17: Steered molecular dynamics (SMD) simulations reveal conformational changes in the cytoplasmic domain of syndecan-4 in response to force on the extracellular domain. a, Syndecan-4 amino acid sequence, where 1-18: signal peptide, 19-145: extracellular domain (green), 146-170: transmembrane domain (brown), 171-198: cytoplasmic domain (purple). Region used in molecular dynamics (MD) and steered molecular dynamics (SMD) simulations is underlined. **b,** Multiple replica SMD simulations at 50 pN. Conformational changes of the cytoplasmic domain of syndecan-4 (upper panel) and sliding of syndecan-4 through the membrane (lower panel) in steered molecular dynamics (SMD) simulations using constant force pulling at 50 pN for 50 ns (4 parallel simulations).
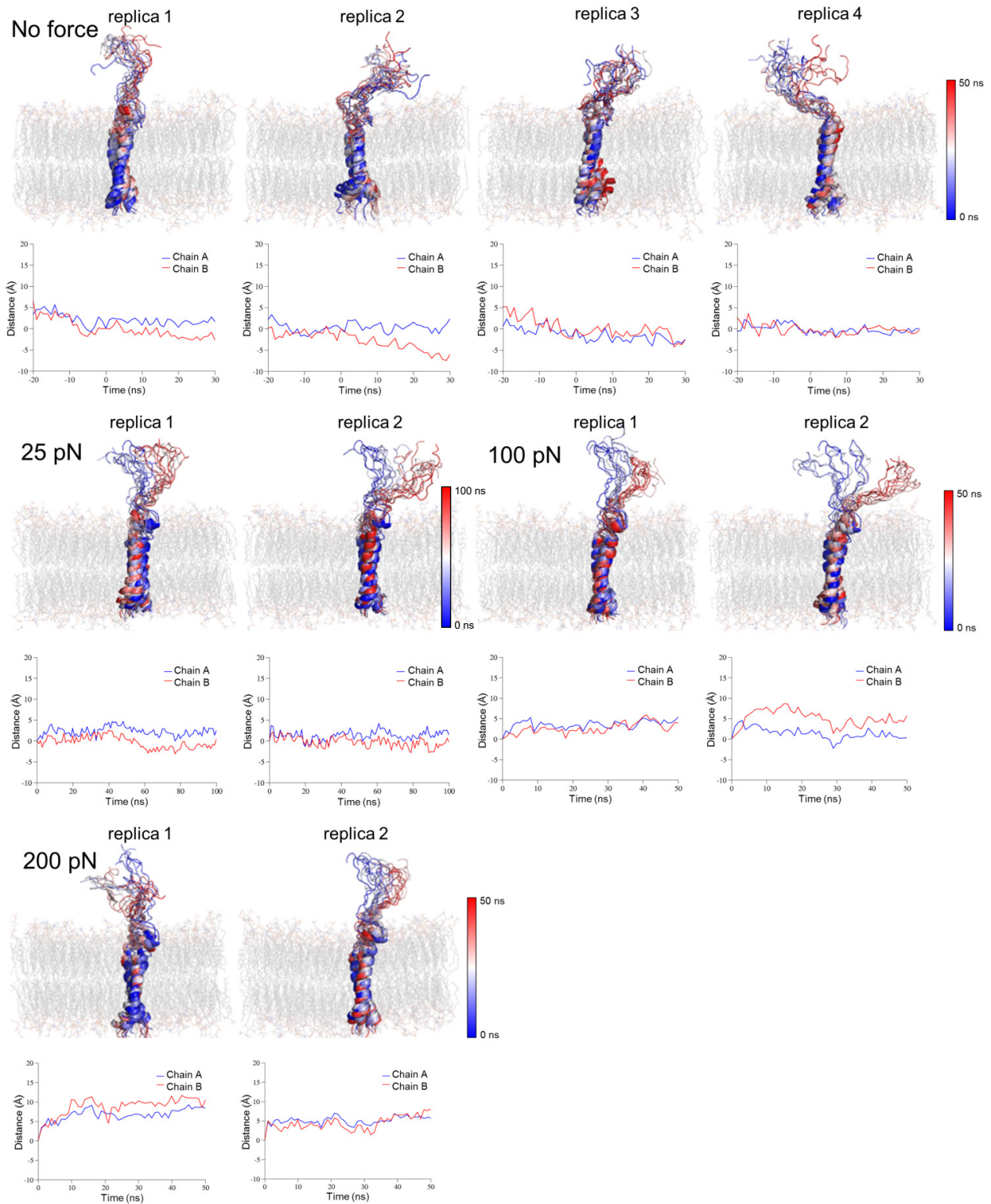
Supplementary Figure 18: Effect of force magnitude on syndecan-4 conformation in molecular dynamics (MD) and steered molecular dynamics (SMD) simulations. Conformational changes of cytoplasmic domain of syndecan-4 (upper panel) and sliding of syndecan-4 through the membrane (lower panel) in MD over 50 ns (No force; 4 parallel simulations) and SMD simulations using constant force pulling at 25 pN for 100 ns (2 parallel simulations), 100 pN for 50 ns (2 parallel simulations) and 200 pN for 50 ns (2 parallel simulations).
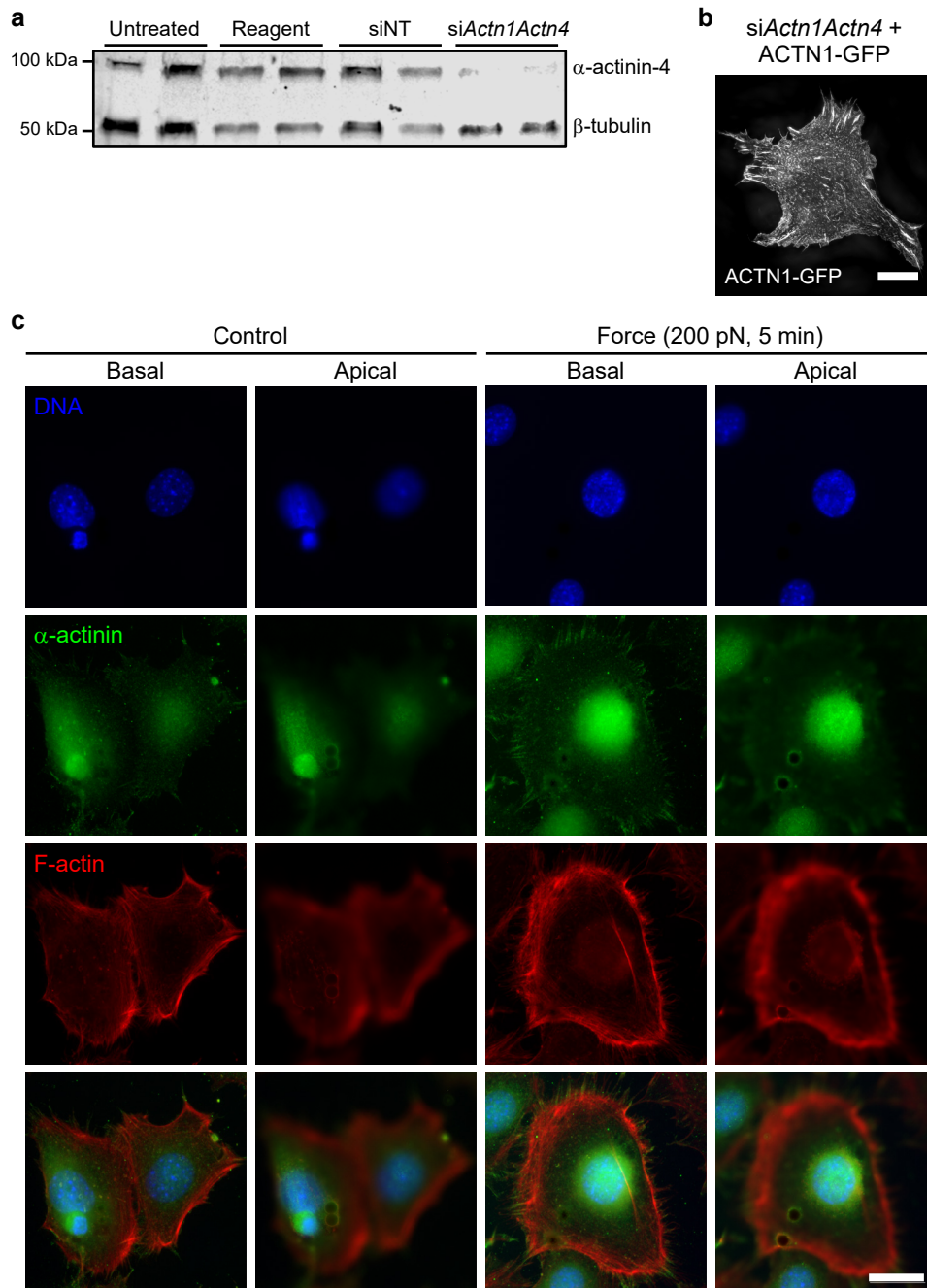
Supplementary Figure 19: α-actinin-1-GFP localises to focal adhesions akin to endogenous α-actinin. a, Western blot demonstrating successful siRNA mediated knockdown of α-actinin-4. Mouse embryonic fibroblasts (MEFs) were untreated, treated with transfection reagent lipofectamine 3000 alone, with a non-targeting control siRNA (siNT), and siRNAs targeting both α-actinin-1 (*Actn1*) and α-actinin-4 (*Actn4*; si*Actn1Actn4*). Duplicate samples presented are representative from 2 biologically independent experiments with similar results. **b,** Representative maximum projection of a 3D super resolution structured illumination microscopy image of α-actinin-1-GFP (ACTN1-GFP) localisation in *Actn1* and *Actn4* depleted MEFs. Note intense localisation to focal adhesions. Image representative of 3 biologically independent experiments with similar results. Scale bar 10 μm. **c,** Representative wide field immunofluorescent images of DNA, F-actin and α-actinin in pancreatic stellate cells under control unstimulated conditions, and in response to sustained 200 pN force for 5 min applied using a permanent magnet to syndecan-4 bound beads. Images were taken at the basal and apical (bead) plane. Note the localisation of α-actinin around the bead adhesion. Images representative of 2 independent experiments with similar results. Scale bar 20 μm.
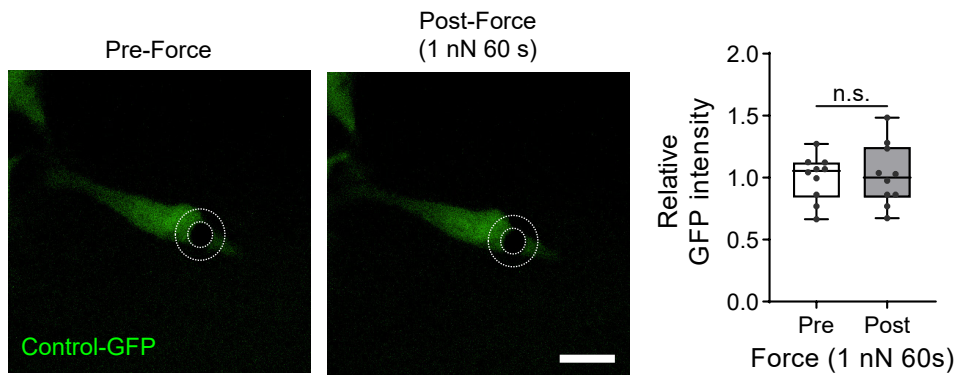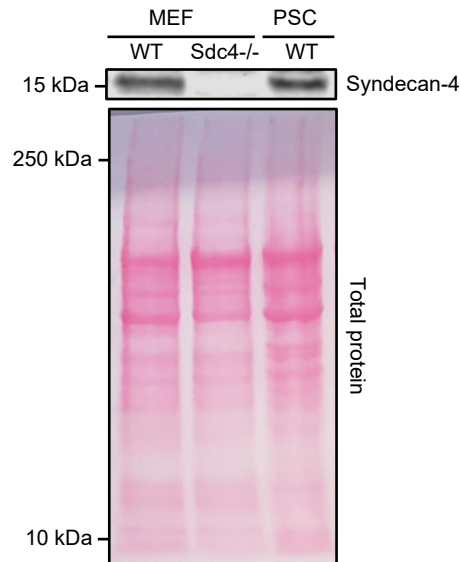
Supplementary Figure 20: Force on syndecan-4 bound beads does not induce control empty vector GFP accumulation in the bead region. Sustained force of 1 nN for 60 s applied to syndecan-4 bound beads on mouse embryonic fibroblasts expressing an empty control GFP vector did not lead to GFP accumulation in the bead region, unlike in cells expressing α-actinin-1 (ACTN1)-GFP (Fig. 6b). Representative images of the area surrounding the magnetic bead pre (0 s) and post (60 s) force application. Mean GFP fluorescent intensity, in a region of interest surrounding the bead depicted by white dashed overlay, is presented relative to mean intensity prior to force application. Scale bar: 10 μm. n = 10 cells; two-sided paired signed rank test: n.s. P = 0.754. Boxes represent median and interquartile range, whiskers extend to the max/min data points, individual values are overlaid.
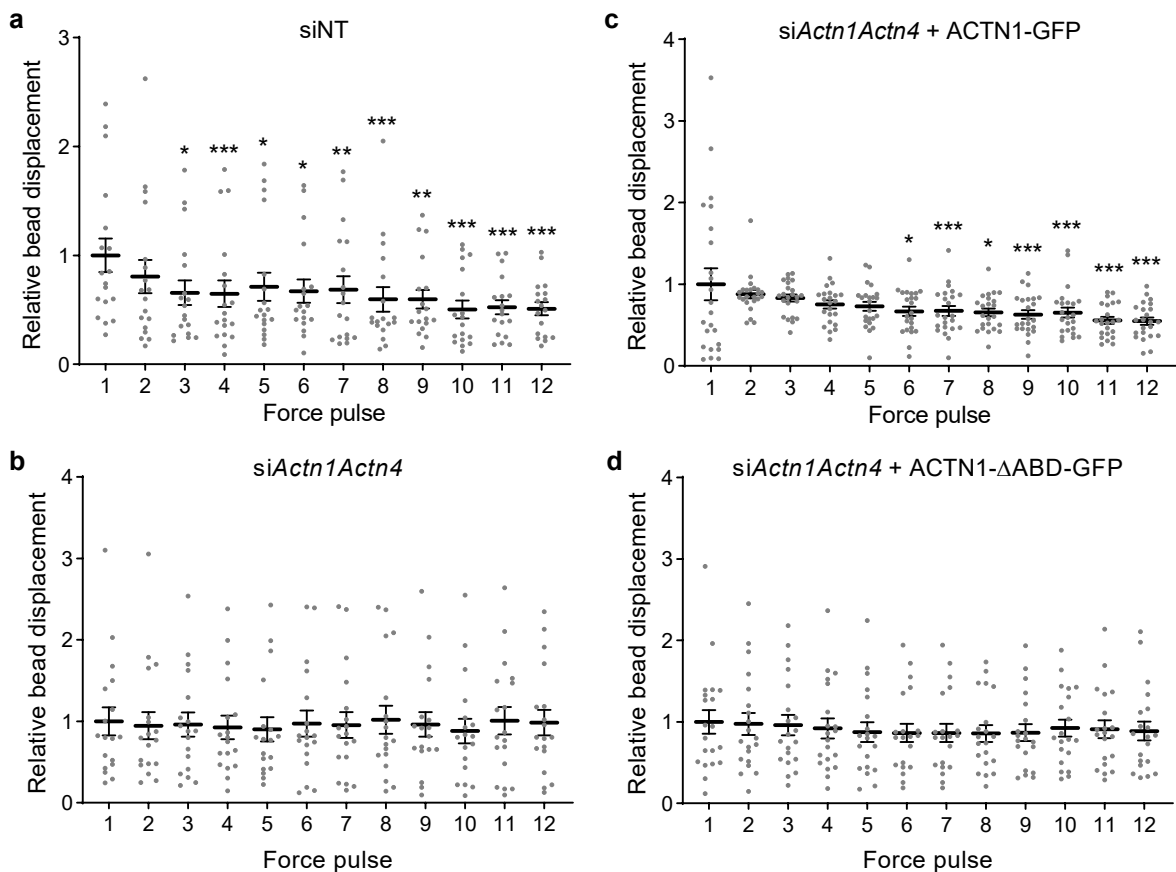

Supplementary Figure 21: Single cell data corresponding to summarised magnetic tweezers bead displacement data presented in Figure 6d. a-d, Bead displacement presented relative to the mean value for force pulse 1 in response to 1 nN pulsatile force applied to syndecan-4 bound beads on mouse embryonic fibroblasts (MEFs) plated on fibronectin. MEFs were treated with (**a**) non-targeting control siRNA (siNT; n = 18) or (**b**) siRNAs targeting α-actinin-1 (*Actn1*) and α-

actinin-4 (*Actn4*; si*Actn1Actn4*; *n* = 18) with expression of (**c**) α-actinin-1 (ACTN1)-GFP (si*Actn1Actn4* + ACTN1-GFP; *n* = 23) or (**d**) a mutant form of α-actinin with the actin binding domain (ABD) deleted (si*Actn1Actn4* + ACTN1-ΔABD-GFP; *n* = 20 cells).; Friedman test with Dunn pairwise comparisons: *$P \leq 0.0492$, **$P \leq 0.0058$, ***$P \leq 0.0009$ vs force pulse 1. Mean ± s.e.m. with individual values overlaid.

Supplementary Figure 22: Syndecan-4 is expressed in wild type (WT) mouse embryonic fibroblasts (MEFs) and pancreatic stellate cells (PSCs) but not in syndecan-4 null (Sdc4-/-) MEFs. Western blot bands for syndecan-4 (Sdc4) and Ponceau-S staining for total protein. Blot representative of 3 independent experimental repeats with similar results. Full syndecan-4 blot is presented in Supplementary Fig. 23.

a Supplementary Figure 2

b Supplementary Figure 19a

c Supplementary Figure 22
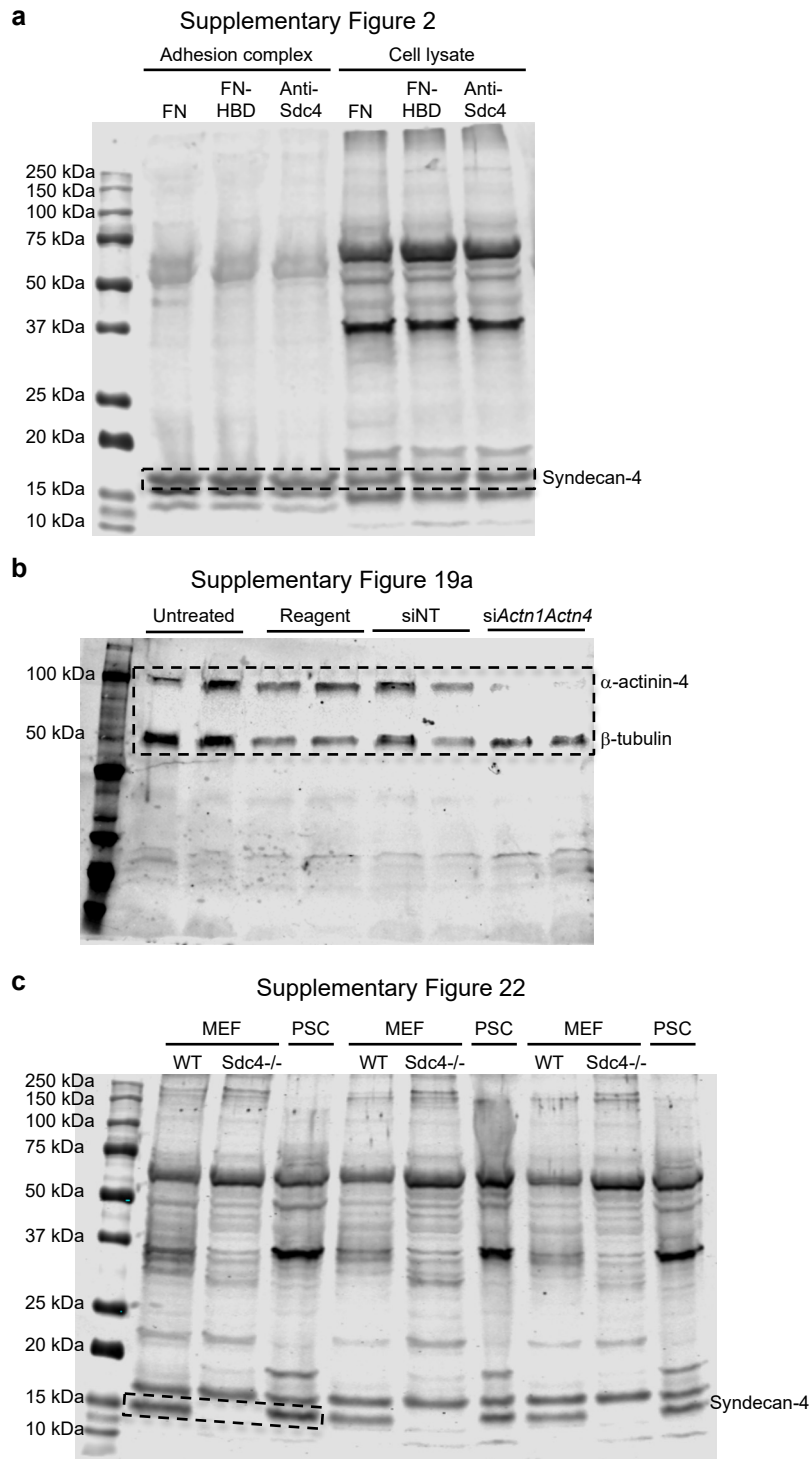
Supplementary Figure 23: Full blot membranes for western blot bands. a-c, Full blot membranes for bands presented in (**a**) Supplementary Fig. 2, (**b**) Supplementary Fig. 19a, and (**c**) Supplementary Fig. 22. In order to resolve syndecan-4 in western blots, heparan sulphate chains were removed through heparinase digestion. Regions presented in respective figures are identified by dashed box.

Supplementary Discussion

Cell-wide integrin activation is triggered by PI3K and leads to subsequent production of freely diffusible PIP_3 phosphoinositides that bind to the PH domain of focal adhesion protein kindlin-2, switching $\beta1$ integrins into a high affinity state to promote ECM ligation. The diffusion rate of PIP_3 is ~0.1-1 $\mu m^2 s^{-1}$ (ref. 1), which is sufficient for the propagation of the biochemical signal to sites distal from that of force application to initiate global activation of integrins within the timescales of our experiments. It is therefore likely that the stiffening response to syndecan-4 mechanosensing represents a global cytoskeletal response rather than a local strengthening of the bead adhesion complex.

Molecular dynamics simulations of tension application to the extracellular domain of syndecan-4 revealed a force-dependent repositioning of the cytoplasmic domain where the V-region moved toward the plasma membrane. This mechanism contrasts with mechanotransduction mechanisms requiring mechanical unfolding of proteins to expose cryptic sites for signalling[2]. This conformation change may facilitate interaction between the V-region and membrane associated PIP_2 which is necessary for PKC-α activation[3], or facilitate α-actinin binding[4]. A direct interaction between the syndecan-4 V-region and α-actinin is a key functional unit that promotes the assembly of focal adhesions and their associated linear microfilament bundles[5]. We have found that force-induced stabilisation of a syndecan-4/α-actinin/F-actin molecular scaffold at the focal adhesion serves as a direct structural link to the cytoskeleton necessary for force transmission and downstream mechanosignalling. α-actinin also associates with integrins, vinculin and zyxin within focal adhesions. It may also possess signalling roles as reports indicate α-actinin interacts with PIP_2 and focal adhesion kinase (FAK)[6]. Force-induced stabilisation of α-actinin at syndecan-4 enriched adhesions may result in recruitment of other essential adhesion components such as zyxin, vinculin and $\beta1$ integrins, to establish cell contraction and downstream syndecan-4 mechanosignalling. Beyond its function to sustain tension across syndecan-4 adhesions, α-actinin may also have direct additional roles in signalling, or indirectly as a force-sensitive scaffold via recruitment of other signalling proteins.

Syndecan-4-mediated force transduction was also found to activate YAP, a major transcriptional regulator and mechanosensor that relays mechanical and cytoskeletal signals to the nucleus. We demonstrate that syndecan-4-mediated tension at the cell-ECM interface is required for nuclear shuttling and activation of YAP and subsequent transcription of downstream YAP target genes. Low matrix tension or attenuated syndecan-4 mechanosignalling causes cytoplasmic YAP retention. The fact that the syndecan-4 null phenotype displays largely deactivated YAP and repressed YAP transcriptional signalling indicates a requirement for ECM ligation and mechanosignalling via both integrins and syndecan-4 to fully activate YAP. The syndecan-4 null phenotype has a distinct cytoskeletal architecture with defects in microfilament assembly and an absence of F-actin stress fibres[5,7], as well as impairments in focal adhesion assembly[5,8]. Presumably, deactivated YAP in syndecan-4 null cells is secondary to lower cytoskeletal tension, owing to deficits in F-actin stress fibre formation and destabilisation of cell-matrix adhesions resulting in decreased RhoA signalling and YAP activity.

Interestingly, a recent study demonstrated a direct kindlin-2-RhoA signalling axis that senses mechanical cues from the cell microenvironment to control YAP and mesenchymal stem cell differentiation[9]. Since syndecan-4 knockout also results in phenotypic disturbances and secondary cytoskeletal impairments[5], we speculate that the mechanical activation of YAP downstream of syndecan-4 may be linked to a RhoA-mediated increase in overall cytoskeletal tension and stress fibre assembly, leaving the possibility for a similar kindlin-2-RhoA axis.

The broader implications for this force-dependent regulation of $\beta1$ integrin activity in stromal fibroblasts downstream of syndecan-4 have yet to be established but likely extend to other cellular processes. For example, fibronectin has binding sites for both integrins and syndecans and a growing body of studies has revealed actomyosin generated forces transmitted through members of the $\beta1$ integrin family play a critical role in fibronectin fibrillogenesis[10]. Also, syndecan family members have been shown to play a role in the architectural regulation of the matrix microenvironment, potentially creating favourable niches for directional migration and cancer metastasis[11]. Thus, stromal syndecan-4 mechanotransduction may modulate the program of fibronectin fibrillogenesis, matrix assembly and overall ECM organisation by regulating integrin-mediated adhesion and actomyosin contraction with important implications for connective tissue homeostasis in health and disease. A stiff fibrotic matrix is a major clinical finding in most solid tumours. While the role of integrin-mediated mechanosignalling has been the subject of intense investigation in the field of cancer mechanobiology in recent years, a more integrative approach that includes syndecan-4 as a key mechanosensor could pave the way for novel insights into disease mechanisms.

Supplementary Methods
Western blotting

Immediately after treatment, cell lysates were prepared in radio immunoprecipitation assay (RIPA) buffer (Sigma-Aldrich R0278) containing protease inhibitors (Sigma-Aldrich 4693124001) and phosphatase inhibitors (Sigma-Aldrich 4906837001). Cell lysates were centrifuged at 16,000 ×g for 20 min, and protein concentration was quantified using a BCA protein assay kit (Fisher Scientific 10678484). In order to resolve syndecan-4 in western blots, heparan sulphate chains were removed through enzymatic digestion. 100 μg total protein was methanol precipitated and suspended in buffer containing 50 mM HEPES, 50 mM NaOAc, 150 mM NaCl, 5 mM $CaCl_2$, ph 6.5 with 4×10^{-3} IU ml^{-1} heparinase I and 2.6 IU ml^{-1} heparinase III (Sigma-Aldrich H3917) for 4 h at 37°C with gentle rotation. Lysate was mixed with 4× Laemmli sample buffer including β-mercaptoethanol, heated at 95°C for 5 min, and 10-20 μg loaded into each well of a 4-20% gel (Mini-PROTEAN TGX, Bio-Rad). For analysis of adhesion complex, cell lysates were prepared from 25 cm^2 flasks in 1% IGEPAL CA-630 (Sigma I8896), 150 mM NaCl, 50 mM Tris, pH 8 buffer containing EDTA-free protease inhibitors (Sigma 11836170001) and phosphatase inhibitors. Following rotation at 4°C for 25 min, beads were isolated from the cell lysate using a magnet. Beads were washed 3 times in lysis buffer and suspended in 2× Laemmli sample buffer containing β-mercaptoethanol, heated at 95°C for 5 min, and bead complex loaded into a 4-20% gel alongside whole cell lysate controls. Separated proteins were transferred onto nitrocellulose membrane (Bio-Rad). Total protein was assessed using Ponceau S stain (Sigma-Aldrich). Following removal of Ponceau S, blots were blocked in Odyssey Blocking Buffer in Tris buffered saline (TBS; Li-Cor) for 1 h. Blots were incubated with primary antibodies diluted in TBS-tween 20 (TBST) at 4°C overnight. Following washes in TBST, blots were incubated with IRDye 680RD or IRDye 800CW conjugated donkey anti-mouse or donkey anti-rabbit secondary antibodies (Li-Cor) at 1:15,000 in TBST for 1 h. After washing in TBST, blots were imaged using an Odyssey infrared imager. Quantification of protein bands was carried out using Image Studio Lite 5.2 (Li-Cor). Primary antibodies: rabbit anti-β-tubulin (1:5,000; Abcam ab15568; RRID:AB_2210952), mouse anti-α-actinin 4, clone G-4 (1:500, Santa Cruz Biotechnology sc-390205; RRID:AB_2797388) and rabbit anti-syndecan-4 (1:500 Abcam ab24511; RRID:AB_448112). Uncropped blots are presented in Supplementary Figure 23.

Supplementary References

1 Hammond, G. R., Sim, Y., Lagnado, L. & Irvine, R. F. Reversible binding and rapid diffusion of proteins in complex with inositol lipids serves to coordinate free movement with spatial information. *J Cell Biol* **184,** 297-308 (2009).

2 del Rio, A. *et al.* Stretching single talin rod molecules activates vinculin binding. *Science* **323,** 638-641 (2009).

3 Bass, M. D. & Humphries, M. J. Cytoplasmic interactions of syndecan-4 orchestrate adhesion receptor and growth factor receptor signalling. *Biochem. J.* **368,** 1-15 (2002).

4 Greene, D. K., Tumova, S., Couchman, J. R. & Woods, A. Syndecan-4 associates with alpha-actinin. *J. Biol. Chem.* **278,** 7617-7623 (2003).

5 Okina, E., Grossi, A., Gopal, S., Multhaupt, H. A. & Couchman, J. R. Alpha-actinin interactions with syndecan-4 are integral to fibroblast-matrix adhesion and regulate cytoskeletal architecture. *Int. J. Biochem. Cell Biol.* **44,** 2161-2174 (2012).

6 Sjoblom, B., Salmazo, A. & Djinovic-Carugo, K. Alpha-actinin structure and regulation. *Cell Mol Life Sci* **65,** 2688-2701 (2008).

7 Gopal, S. *et al.* Heparan sulfate chain valency controls syndecan-4 function in cell adhesion. *J. Biol. Chem.* **285,** 14247-14258 (2010).

8 Cavalheiro, R. P. *et al.* Coupling of vinculin to F-actin demands Syndecan-4 proteoglycan. *Matrix Biol.* **63,** 23-37 (2017).

9 Guo, L. *et al.* Kindlin-2 regulates mesenchymal stem cell differentiation through control of YAP1/TAZ. *J Cell Biol* **217,** 1431-1451 (2018).

10 Schwarzbauer, J. E. & DeSimone, D. W. Fibronectins, their fibrillogenesis, and in vivo functions. *Cold Spring Harb Perspect Biol* **3,** 1-19 (2011).

11 Yang, N., Mosher, R., Seo, S., Beebe, D. & Friedl, A. Syndecan-1 in breast cancer stroma fibroblasts regulates extracellular matrix fiber organization and carcinoma cell motility. *Am J Pathol* **178,** 325-335 (2011).